

FINAL REPORT

Advanced UXO Discrimination using Magnetometry: Understanding Remanent Magnetization

SERDP Project MM-1380

SEPTEMBER 2009

Stephen Billings
Sky Research, Inc.

This document has been approved for public release.



Strategic Environmental Research and
Development Program

This report was prepared under contract to the Department of Defense Strategic Environmental Research and Development Program (SERDP). The publication of this report does not indicate endorsement by the Department of Defense, nor should the contents be construed as reflecting the official policy or position of the Department of Defense. Reference herein to any specific commercial product, process, or service by trade name, trademark, manufacturer, or otherwise, does not necessarily constitute or imply its endorsement, recommendation, or favoring by the Department of Defense.

Advanced UXO Discrimination Using Magnetometry:UX-1380 Final Report
 Understanding Remanent Magnetization

REPORT DOCUMENTATION PAGE			Form Approved OMB No. 0704-0188
<small>Public reporting burden for this collection of information is estimated to average 1 hour per response, including the time for reviewing instructions, searching existing data sources, gathering and maintaining the data needed, and completing and reviewing the collection of information. Send comments regarding this burden estimate or any other aspect of this collection of information, including suggestions for reducing this burden, to Washington Headquarters Services, Directorate for Information Operations and Reports, 1215 Jefferson Davis Highway, Suite 1204, Arlington, VA 22202-4302, and to the Office of Management and Budget, Paperwork Reduction Project (0704-0188), Washington, DC 20503.</small>			
1. AGENCY USE ONLY (Leave blank)	2. REPORT DATE 09-30-2009	3. REPORT TYPE AND DATES COVERED Draft Final Technical Report. 2004-2009	
4. TITLE AND SUBTITLE Project MM-1380: Advanced UXO Discrimination using Magnetometry Understanding Remanent Magnetization Draft Final Report		5. FUNDING NUMBERS UX-1380	
6. AUTHOR(S) Stephen Billings, Yaoguo Li, Whitney Goodrich			
7. PERFORMING ORGANIZATION NAME(S) AND ADDRESS(ES) Sky Research, Inc. 445 Dead Indian Memorial Road Ashland, OR 97520		8. PERFORMING ORGANIZATION REPORT NUMBER	
9. SPONSORING/MONITORING AGENCY NAME(S) AND ADDRESS(ES) Strategic Environmental Research and Development Program 901 North Stuart Street, Suite 303 Arlington, VA 22203-1821		10. SPONSORING/MONITORING AGENCY REPORT NUMBER	
11. SUPPLEMENTARY NOTES			
12a. DISTRIBUTION/AVAILABILITY STATEMENT Unclassified/Unlimited		12b. DISTRIBUTION CODE	
13. ABSTRACT (Maximum 200 words) The use of apparent magnetic remanence to prioritize the digging order at sites contaminated by unexploded ordnance was investigated. A mobile device for measuring the magnetic remanence of field samples was constructed and deployed to two field sites and to make before firing and after impact measurements of 81 mm mortars at a test-facility. Results from the field sites indicated that most, but not all, excavated ordnance items had small remanent magnetization, suggesting that shock demagnetization occurs. The controlled firing tests proved that shock demagnetization occurred and also demonstrated that initially demagnetized rounds acquire a remanent magnetization in the direction of the inducing field at the time of impact. Shock demagnetization of highly magnetized 81 mm mortars was not sufficient to guarantee the success of a ranking scheme based on apparent remanence, so we conclude that the method should not be used if 100% recovered of detected UXO is required. Apparent remanence does provide an efficient ranking scheme for recovery of 95% of UXO. Measurements of the magnetic viscosity of steel samples revealed that magnetic remanence is stable on time-scales of at least 1000 years and is not a significant factor that needs to be considered from a discrimination perspective.			
14. SUBJECT TERMS Magnetic Remanence; UXO		15. NUMBER OF PAGES 82	
		16. PRICE CODE	
17. SECURITY CLASSIFICATION OF REPORT Unclassified	18. SECURITY CLASSIFICATION OF THIS PAGE Unclassified	19. SECURITY CLASSIFICATION OF ABSTRACT Unclassified	20. LIMITATION OF ABSTRACT Unlimited

Acknowledgements

This technical report for project UX-1380, "*Advanced UXO Discrimination using Magnetometry: Understanding Remanent Magnetization:*" documents the results of field measurements and theoretical studies undertaken to further the understanding of remanent magnetization in relation to munitions, and in particular, whether it can be used to discriminate between UXO and munitions scrap or shrapnel. The work was performed by Sky Research, Inc and the University of British Columbia-Geophysical Inversion Facility. Dr Stephen Billings from Sky Research was the principal investigator.

Funding for this project was provided by the Strategic Environmental Research and Development Program Office. We wish to express our sincere appreciation to Dr. Jeffrey Marqusee, Dr. Anne Andrews, Dr. Herb Nelson, and staff of the SERDP Office for providing support and funding for this project. We would also like to thank Larry Overbay and staff at the Aberdeen Test Center for providing support for the firing tests conducted in support of this research, and to Dr Clif Youmans and the Montana Army National Guard for assistance with the field measurements at Limestone Hills.

This report was prepared under contract to the Department of Defense Strategic Environmental Research and Development Program. The publication of this report does not indicate endorsement by the Department of Defense, nor should the contents be construed as reflecting the official policy or position of the Department of Defense. Reference herein to any specific commercial product, process, or service by trade name, trademark, manufacturer, or otherwise, does not necessarily constitute or imply its endorsement, recommendation, or favoring by the Department of Defense.

Executive Summary

The apparent remanence discrimination method developed at the University of British Columbia was successfully applied to sites in Montana, resulting in false-alarm rates between 1 and 5 non-UXO for each excavated UXO item. In the apparent remanence method, the amount of remanent magnetization in recovered dipole moments of collected magnetic data is estimated and a prioritized dig-list is developed based on the assumption that items with lower remanence are more likely to be UXO. There were differences in the apparent remanent magnetization of seeded and live-site UXO evident in the Montana case-studies, indicating that our conceptual understanding of remanence in UXO was incomplete. As the discrimination technology would result in certain detected items being left in the ground, a comprehensive understanding of the physical phenomena was deemed necessary. This was the impetus for this project.

As part of this project we developed a mobile device, the Magnetic Remanence Interrogation Platform (MRIP), for measuring the induced and remanent moments of steel samples. The MRIP comprises six three-component fluxgate magnetometers symmetrically distributed around a rotating sample holder. Samples are placed on the holder and are slowly spun through two complete rotations. The measurement is repeated after the sample is physically rotated by 90° so that the previous up direction points east. The MRIP platform was deployed to two field sites (Limestone Hills and Camp Sibert), as well as to the Aberdeen Test Center where measurements were made on 81 mm mortars before and after firing. At Limestone Hills the one-hundred and forty-nine 76- and 90-mm projectiles were measured. Most had relatively low remanent magnetization relative to the induced, suggesting that shock demagnetization occurs. Variations in the remanent moments of different specimens of 90-mm projectiles were attributed to variations in the type of steel used. There was a strong correlation of the direction of remanent and inducing field during burial, indicating evidence of shock magnetization and/or magnetic viscosity. At the second site, intact and partial 4.2-in mortars as well as shrapnel, base plates, and cultural debris were measured. Most of the base plates and intact mortars had low remanent magnetization, whereas the shrapnel and partial mortars tended to have higher remanent magnetization.

At ATC the MRIP device was used to make measurements of the magnetic remanence of sixty-five 81 mm mortars before firing and after impact. As delivered, 64 of the 65 rounds had very low remanent magnetization and a magnetizer had to be used to impose various amounts of remanence on the mortars. Three different categories of initial remanent magnetization were created (low, medium and high remanence) and these were fired at three different charge increments (0, 1 and 2 charge increments). The mortars that initially had low remanent magnetization acquired a magnetization in the direction of the inducing field, with the amount of shock magnetization decreasing with increasing impact velocity. The mortars with medium and high initial magnetization all lost some of their magnetic remanence with the amount increasing with increasing impact velocity (from ~50% at 0 charge increment to ~70% at two charge increments). Even at the highest impact velocity, shock demagnetization of initially highly magnetized mortars was insufficient to guarantee effective discrimination using apparent remanence.

During the project, two visits were made to the Institute of Rock Magnetism for the purpose of measuring the magnetic properties (in particular the magnetic viscosity) of a number of steel samples. The magnitude of magnetic viscosity for fresh steel, unfired projectiles, unexploded ordnance, and shrapnel was quite similar at less than 1.5% decay for the time scale of interest for the MRIP, and less than 6% decay for all time brackets up to 1000 years with an average of 3.38% decay. The viscous decay of the unfired projectiles was slightly higher than that of the UXO, shrapnel, and fresh steel, but only by about 2%. In short, magnetic remanence persists longer than the time scales of interest. It is stable for time scales of up to one thousand years, quite likely even longer. For this study the magnetic viscosity will not hinder the ability of the MRIP to resolve the magnetic remanence of a given UXO. In addition, the results of this experiment have an important implication; magnetic viscosity is not relevant to the magnetic discrimination process.

The main conclusion of this project is that **discrimination using apparent remanence is not reliable enough to guarantee the excavation of all detected UXO**. In the live-site measurements at Camp Sibert and the controlled firing tests at ATC several ordnance items possessed sufficient magnetic remanence to confound the apparent remanence metric ranking scheme. The measurements made at Limestone Hills suggest that apparent remanence might be more reliable for direct fired artillery projectiles that presumably suffer a larger shock on impact. However, even at Limestone Hills, there was a least one outlier with relatively high magnetic remanence. Therefore, we can never guarantee that sufficient demagnetization occurs so that apparent remanence discrimination will be reliable. There is simply too much potential variability in both the initial magnetic remanence and shock regime experienced by a projectile.

The Limestone Hills and Camp Sibert field measurements, along with the earlier Montana case-studies, demonstrate that apparent remanence is an effective method to recover 95% or more of the unexploded projectiles without the need to excavate all the detected shrapnel, range debris and cultural junk. Thus apparent remanence could provide an effective ranking strategy in applications where not all detected anomalies can be excavated. This includes marine applications where the expense of excavating a single anomaly typically prevents all detected anomalies from being investigated. Another application is in the interpretation of HeliMAG data or ground based transects collected for wide-area-assessment purposes.

Summarizing other relevant results from this study:

- 1) **Shock demagnetization:** The controlled firing tests at ATC demonstrate that Altshuler's (1996) hypothesis that shock demagnetization occurs in ordnance was correct. As intuitively expected the amount of demagnetization increases with increasing impact shock. However, the maximum impact velocity achieved at ATC (210 m/s) was insufficient to completely erase the preexisting remanence of the 81 mortars that had a high initial magnetic remanence.
- 2) **Shock magnetization:** The controlled tests at ATC conclusively demonstrated that shock magnetization of rounds occurs. Rounds that initially started with a very small remanence acquired a magnetic remanence in the direction of the inducing field at the time of impact.
- 3) **Magnetic viscosity:** The measurements made at the IRM indicate that magnetic remanence is stable for time scales of up to one thousand years, quite likely even longer, indicating that magnetic viscosity is not relevant to the magnetic discrimination process.

Table of Contents

ACKNOWLEDGEMENTS	I
EXECUTIVE SUMMARY	II
LIST OF FIGURES	V
LIST OF TABLES	VI
1. PROJECT BACKGROUND AND OBJECTIVES	1
2. DEVELOPMENT OF AN INSTRUMENT FOR MEASURING REMANENT MAGNETIZATION (TASK 1)	3
3. MEASUREMENT OF THE MAGNETIC REMANENCE OF MUNITIONS PRE- AND POST- FIRING AT A TEST RANGE (TASK 2)	4
3.1. SELECTION OF TEST-ROUNDS	4
3.2. TEST MATRIX	5
3.3. MEASUREMENT PROCEDURE	7
3.3.1. <i>Location of firing tests</i>	<i>8</i>
3.3.2. <i>MRIP measurement procedure</i>	<i>9</i>
3.3.3. <i>Magnetization of rounds prior to firing</i>	<i>10</i>
3.4. <i>Results</i>	<i>11</i>
3.5. <i>Discussion and Conclusions</i>	<i>21</i>
4. MEASUREMENT OF THE REMANENT PROPERTIES OF UXO AND SHRAPNEL IN THE FIELD (TASK 3)	22
5. DEVELOPMENT OF A THEORETICAL OR EMPIRICAL MODEL OF SHOCK INDUCED CHANGES TO MAGNETIZATION (TASK 4)	22
6. COLLECTION OF TEST-STAND DATA OVER MUNITIONS (TASK 5)	22
7. INCORPORATION OF MAGNETIC DISCRIMINATION METHODS INTO A WORKABLE SOFTWARE SYSTEM (TASK 6)	22
8. MEASUREMENT OF VISCOUS REMANENT MAGNETIZATION AT THE INSTITUTE FOR ROCK MAGNETISM (TASK 7)	24
8.1. THEORETICAL MODEL	28
8.2. MEASUREMENT PROCESS	30
9. SUMMARY AND CONCLUSIONS	43
9.1. SUMMARY	43
9.2. CONCLUSIONS	44
10. REFERENCES	46
APPENDIX A: FIELD DIARY FOR ATC FIRING TESTS	48
APPENDIX B: THEORY OF SHOCK INDUCED CHANGES TO MAGNETIZATION	51

List of Figures

Figure 1. Remanent magnetization of 76 and two types of 90 mm projectiles measured with the MRIP platform at Limestone Hills, MT. Remanent magnetizations are split into the component along the axis of the project (axial) and across the axis (perpendicular). Contours delineating the values of the induced magnetizations of the 76 and 90 mm projectiles (as previously measured at the U.S. Army Corps of Engineers (USACE) Engineer Research and Development Center (ERDC) test stand) are also shown. The axial induced magnetization for the 90 mm projectile larger than the range of values shown on the plot.	6
Figure 2. Location of the firing tests on the I-field site at Aberdeen Proving Ground.....	9
Figure 3. Example hysteresis curve.	10
Figure 4. The Magnaflux A940 which is similar in appearance, although considerably smaller, than the Magnaflux H-6472 model we used (a photo was not available).	11
Figure 5. Change in remanence after firing and impact for (a) charge 0; (b) charge 1; and (c) charge 2. The two dashed black circles delineate the transverse and axial induced magnetizations for the 81 mm mortar. A grey line joins the before firing and after impact values for a given item.....	16
Figure 6. Zoomed in view of the change in remanence after firing and impact for (a) charge 0; (b) charge 1; and (c) charge 2. A grey line joins the before firing and after impact values for a given item. Also shown on this plot are contour that delineate the regimes where apparent remanence is always less than 50% and 75%.....	17
Figure 7. Change in remanence after firing and impact for (a) charge 0; and (b) charge 1, with remanent moments split into components parallel and perpendicular to the induced field at the time of impact. A grey line joins the before firing and after impact measurements for a given item.	18
Figure 8. Cummulative histograms of apparent remanence for rounds before and after firing. The results are presented separately for the different charge increments (as columns) and for difference amounts of initial remanence (low, medium and high are top, middle and bottom rows respectively).	19
Figure 9. Apparent remanence in the ‘as found’ orientation for before firing and after impact.....	20
Figure 10. Linear model of the change in remanence for the mortars fired at different change increments: (a) compares axial remanence; (b) compares transverse remanence, while (c) compares the magnetization in the direction of the induced magnetization at the time of impact (charge 2 results not shown as no orientation measurements were made), with (d) the results for the remanence perpendicular to the inducing field.....	21
Figure 11. Low carbon steel bar from which samples were obtained.	24
Figure 12. Samples cut from low carbon steel bar.	25
Figure 13. Unfired 81 mm M821/M889 mortar HE.....	25
Figure 14. Unfired 120 mm M1 HE.....	25
Figure 15. Sample from unfired 81 mm M821/M889 mortar HE.....	26
Figure 16. Samples from Unfired 120 mm M1 HE.....	26
Figure 17. Unexploded ordnance - 81 mm mortar.	27
Figure 18 Unexploded ordnance - 90 mm M353 target practice round.....	27
Figure 19. Unexploded 90 mm M353 projectile samples.	27
Figure 20. Unexploded 81 mm mortar samples.	28
Figure 21. Shrapnel samples from Limestone Hills.....	28
Figure 22. Magnetic viscosity measurements for shrapnel sample C3.....	31
Figure 23. Hysteresis loop of shrapnel sample C3.....	32
Figure 24. Viscous remanent decay for shrapnel sample R2.....	33
Figure 25. Viscous remanent magnetization for paramagnetic sample P2.	34
Figure 26. Cole-Davidson fit to magnetic viscosity measurements for sample Bar 3.....	35
Figure 27. Hysteresis loop for fresh steel sample Bar 3 with a maximum applied field of 250 mT (199 kA/m).....	36
Figure 28. Magnetic viscosity meausements for sample S1-UN-2.....	37

Figure 29. Hysteresis loop for unfired projectile sample 81-UN-2 with a maximum applied field of 1 T (796 kA/m).....38
 Figure 30. Magnetic viscosity measurements for unfired projectile sample 105-UN-2.....38
 Figure 31. Magnetic viscosity measurements of unexploded ordnance sample 90-UXO-3.39
 Figure 32. Hysteresis loop for unexploded ordnance sample 90-UXO-2 with a maximum applied field of 250 mT (=199kA/m).....40
 Figure 33. Magnetic viscosity measurements of unexploded ordnance sample C3.....41

List of Tables

Table 1. Test-matrix showing parameters that were varied. The numbers in brackets are the actual numbers achieved in each category.6
 Table 2. Flight characteristics for the M879 mortars7
 Table 3. Magnetic remanence of rounds as delivered, before firing and after impact.12
 Table 4. Orientations and depths of recovered items.14
 Table 5. Parameters of the linear models in Figure 10.....20
 Table 6. Hysteresis parameters for steel shrapnel samples.....30
 Table 7. Projected decay times of magnetic remanence for shrapnel sample C3.32
 Table 8. Projected decay times of magnetic remanence for shrapnel sample R2.33
 Table 9. Hysteresis parameters for fresh steel, unfired projectile, and unexploded ordnance samples.35
 Table 10. Projected decay times for fresh steel sample Bar 3 using the Cole-Davidson model.....36
 Table 11. Projected decay times of magnetic remanence for unfired projectile sample 81-UN-2 using the Cole-Davidson model.37
 Table 12. Projected decay times of magnetic remanence for unexploded ordnance sample 90-UXO-3 using the Cole-Davidson model.....40
 Table 13. Projected decay times of magnetic remanence for shrapnel sample C3 using the Cole-Davidson model.....41

Acronyms

Am ²	Ampere-meter ²
A/m	Ampere/meter
APG	Aberdeen Proving Ground
AP/T	Armor piercing tank
ATC	Aberdeen Test Center
C	Centigrade
cm	Centimeter
DC	Direct Current
ERDC	Engineer Research and Development Center
HE	High Explosive
Hz	Hertz
IRM	Institute for Rock Magnetism
kg	Kilograms
m	Meter
mm	Millimeter
MRIP	Magnetic Remanence Interrogation Platform
mT	milliTesla
NDE	Non-destructive Evaluation
nT	nanoTesla
PAR VSM	Princeton Applied Research Vibrating Sample Magnetometer
PMC MM	Princeton Measurements Corporation Micro Mag Vibrating Sample Magnetometer
TP-T	Target Practice with a Tracer
UBC-GIF	University of British Columbia-Geophysical Inversion Facility
USACE	United States Army Corps of Engineers
UXO	Unexploded Ordnance
VRM	Viscous Remanent Magnetization
VSM	Vibrating Sample Magnetometer
WP	White Phosphorus

1. Project Background and Objectives

The most well-established techniques for munitions detection are magnetics and electromagnetics. These methods are very effective at locating buried metallic objects such as unexploded ordnance (UXO). However, discriminating between intact UXO and non hazardous objects such as metallic debris and shrapnel is a significant challenge. Often little or no effort is invested in discrimination and consequently many holes are typically excavated for each munitions item recovered.

The principal of magnetic detection is that buried steel munitions items cause a distortion in the Earth's magnetic field that can be measured by a magnetometer. However, magnetic anomalies also arise from shrapnel and other ferrous debris in an area, as well as from geological variations in ferromagnetic materials. To distinguish between the intended munitions item and clutter or geology, a diagnostic feature of the magnetic anomaly of a munitions item must be determined. Ideally, we would like to be able to recover the shape and size of the anomaly's source and use that information for discrimination. However, a fundamental ambiguity in magnetics whereby any magnetic anomaly can be represented by an equivalent layer of susceptibility dooms such a procedure to failure.

To proceed, we note that the response of a compact body can be decomposed into a series of moments by a multi-pole expansion (Stratton, 1941). In most cases, measurements are made in the far-field of the object (i.e. at distances several times the object's dimensions) so that the response of the dipole component dominates due to the rapid decay with distance of the other components. Therefore, all that we can usually recover about a buried object is its dipole moment. In general, an object's dipole moment is a consequence of both remanent and induced magnetization. Remanent magnetization is present even in the absence of an inducing field and is due to ferromagnetic domains in the steel being locked into alignment sometime during the object's history. Induced magnetism arises because magnetic domains in a ferrous material tend to align with the direction of the ambient field.

The remanent magnetic discrimination method developed at the University of British Columbia-Geophysical Inversion Facility (UBC-GIF) has proven successful at sites in Montana resulting in false-alarm rates between 1 and 5 non-UXO for each excavated UXO. Magnetic data from each anomaly are inverted to produce an initial dipole model. This recovered dipole model is then compared to a family of induced magnetic responses of all munitions items suspected at the site. This comparison process defines an apparent remanent magnetization for each target in the library and allows a discrimination ranking criteria to be established (Billings et al. 2002; Billings 2004). The premise of correlating the likelihood of targets being UXO with low magnetic remanence was tested at the Montana sites and was shown to be highly reliable (Billings 2004). Altshuler (1996) postulated that the shock of impact partially erases the remanent magnetization of a UXO item. They further noted that the direction of induced magnetization in typical munitions items is constrained to lie within about 60° of the Earth's field. This fact has been utilized for munitions discrimination with some success (Nelson et al. 1998).

Due to shock demagnetization, UXO items in the munitions library will have low values of apparent remanence. Geological anomalies, shrapnel and other metallic debris will, in general, not match the

induced model very well and hence will have large values of apparent remanence. However, differences in the apparent remanent magnetization of seeded and live-site UXO indicated that our conceptual understanding of remanence in UXO is incomplete. As we are proposing to use a discrimination technology that will leave certain detected items in the ground, a comprehensive understanding of the physical phenomena behind the method is required for it to be reliably extended to other DoD sites.

Therefore, the objective of Project UX-1380 is to improve our fundamental understanding of magnetic remanence and shock effects in UXO. The project was separated into the following six tasks:

- Development of mobile magnetometer systems for measuring magnetic remanence in the field (to build a working magnetic remanence knowledge base);
- Measurement of the magnetic remanence of munitions pre- and post-firing at a test range (to understand shock-demagnetization phenomenology);
- Measurement of the magnetic remanence of UXO and shrapnel at two field sites (to ensure theoretical measurements are consistent with real-world observations);
- Development of a theoretical or empirical model of shock induced changes to magnetization (for predicting the size of remanent magnetization in different munitions items);
- Collection of test-stand data over munitions (for validation of the magnetic modeling approach); and
- Incorporation of magnetic discrimination methods into a workable software system (for transition of technology to the UXO clearance industry).
- After the Interim Progress Review in 2005, we added an extra task (task 7) which was to measure the magnetic viscosity and hysteresis of a number of steel samples.

During the course of this project several papers were published in peer-reviewed journals. Rather than providing a second write-up of the results in this final report, we instead direct the reader to the published papers and include the abstracts in this report:

- Tasks 1 and 3: Billings, S. D., 2009, Field measurements of induced and remanent moments of unexploded ordnance and shrapnel: IEEE Transactions of Geoscience and Remote Sensing, 47, 815-827.
- Task 5: Billings, S. D., Pasion, C, Walker, S. and Beran, L., 2006, Magnetic models of unexploded ordnance: IEEE Transactions of Geoscience and Remote Sensing, 44, 2115-2124.
- Task 6: Billings, S. D. and Youmans, C., 2007, Experiences with unexploded ordnance discrimination using magnetometry at a live-site in Montana: Journal of Applied Geophysics, 61, 195-205.

In addition, the shock modeling results are compiled in a separate report (Trinchenko et al. 2009). The main focus of this report is on understanding the implications of the various field and controlled firing measurements on the viability of a discrimination method based on the apparent remanence metric. The physical mechanism behind shock induced changes in magnetization is described in the Trinckenko et al. (2009) report.

2. Development of an Instrument for Measuring Remanent Magnetization (Task 1)

This task culminated in the development of the Magnetic Remanence Interrogation Platform (MRIP). The design is described in more detail in Billings (2009). The abstract for this paper follows.

“Magnetometry is a widely used technique for clearance of areas contaminated with unexploded ordnance. The discrimination of hazardous ordnance from nonhazardous items is possible using apparent remanence if ordnance is shock demagnetized on impact with the ground. We developed a mobile device, the Magnetic Remanence Interrogation Platform (MRIP), for measuring the induced and remanent moments of steel samples. The MRIP comprises six three-component fluxgate magnetometers symmetrically distributed around a rotating sample holder. Samples are placed on the holder and are slowly spun through two complete rotations. The measurement is repeated after the sample is physically rotated by 90° so that the previous up direction points east. The MRIP platform was deployed to two field sites. At the first site, 76- and 90-mm projectiles were measured. Most had relatively low remanent magnetization relative to the induced, suggesting that shock demagnetization occurs. Variations in the remanent moments of different specimens of 90-mm projectiles were attributed to variations in the type of steel used. There was a strong correlation of the direction of remanent and inducing field during burial, indicating evidence of shock magnetization and/or magnetic viscosity. At the second site, intact and partial 4.2-in mortars as well as shrapnel, base plates, and cultural debris were measured. Most of the base plates and intact mortars had low remanent magnetization, whereas the shrapnel and partial mortars tended to have higher remanent magnetization. The results indicate that there is an inherent risk in using apparent remanence for discrimination as not all ordnance is demagnetized on impact.”

3. Measurement of the Magnetic Remanence of Munitions Pre- and Post-Firing at a Test Range (Task 2)

Through this project we are attempting to understand shock-induced changes to magnetization that occur when a round hits the ground and fails to explode. A portable “Magnetic Remanence Interrogation Platform” (MRIP) was constructed in 2006 and used to measure the remanent magnetization of recovered 76 and 90 millimeter (mm) projectiles at Limestone Hills, MT, and seeded 4.2 inch mortars, shrapnel and range and cultural debris at the Former Camp Sibert, AL. In this section of the report we describe an experiment conducted at the Aberdeen Test Center (ATC), where the remanent magnetization of sixty-five 81 mm mortars were measured both before and after-firing in a series of controlled tests. We had originally planned to take equivalent measurements on 105 mm projectiles, but logistical and scheduling issues prevented those tests from being conducted.

The ATC firing tests were intended to answer the following open questions:

- 1) To what extent does shock demagnetization erase the remanent magnetization of ordnance?
- 2) Do ordnance acquire a shock remanent magnetization when they impact the ground?
- 3) How does impact velocity affect the amount of shock demagnetization that occurs?
- 4) Will rounds with extremely large remanent magnetization undergo sufficient shock demagnetization to be correctly classified using the apparent remanence method?

3.1. Selection of test-rounds

Following a planning meeting at ATC in April 2005, ATC conducted a study to identify projectiles that could be used for pre and post-fire/impact analysis of the magnetic fields of projectiles that could be used for firing tests to be conducted at the Aberdeen Proving Ground (APG). A moderate and large-sized explosive (UXO application) round was sought that had, or could easily be converted to, an inert counterpart. The size and configuration had to be such that magnetic field readings could easily be taken. Another consideration was that the rounds have trajectories and impact velocities that would enhance recoverability and minimize test setup costs. By analyzing assembly, geometry, mass, trajectory characteristics and expected penetration depths, two candidate projectiles were identified for a pre/post-fire magnetization study.

An acceptable candidate for a moderate sized test round was easily identified. The M889A1 mortar cartridge is a common round with an inert target practice counterpart which is the M879 cartridge. The empty mass of the M879 is 3.3 kilograms (kg). The abundant use of the M879 round makes it easily attainable for testing. Further, mortar firing systems are easily setup, their rounds typically have small dispersions, and associated penetration depths are small. Use of an M879 round would therefore facilitate a low test cost with good recoverability potential.

Charge increments and firing elevations were selected for the M879 to provide a variety of launch and impact shocks. Expected remanence performance data and projectile flight characteristics are shown in Tables 1 and 2. Once on site we discussed the firing plan with the firing team and they

indicated that it would not be possible to fire the rounds with 4 charge increments. They recommended a maximum of 2 charge increments, which turned out to be very fortunate as those rounds penetrated at least 8 feet into the ground.

3.2. Test matrix

Within the envisioned measurement scenario we are able to vary:

- 1) Impact velocity; and
- 2) Remanent magnetization of the items prior to firing.

We had hoped to vary the firing trajectory to investigate the difference between direct and indirect fired rounds but the complexity and cost of recovering direct fired rounds was too great for this study.

An axi-symmetric ordnance item has a much larger induced magnetization in the axial direction, m_a , then in the transverse direction m_t (e.g. induced magnetization contours in Figure 1). From prior measurements of similar sized rounds we expected $m_t = 0.07$ amperes-meter² (Am^2) and $m_a = 0.24$ Am^2 for the 81 mm mortar (Billings *et al.*, 2006). Once the rounds were measured we were able to more precisely define these numbers ($m_t = 0.0826$ Am^2 and $m_a = 0.375$ Am^2).

With the magnetic remanence method of Billings (2004) a round is considered a UXO if the apparent remanence is $< 50\%$ (although typically a larger cutoff is used to account for uncertainty in the recovered dipole moment). As shown in Table 2, we planned to use three categories of remanence which we defined as follows:

- 1) Low remanence, which we define as $m_r < m_t/3$: Roughly speaking, we would consider a remanence, m_r , of less than $m_t/3$ to be small. Even if no shock demagnetization occurred, the apparent remanence, as measured from a total-field survey, would never be larger than 50% ¹ so the item should be correctly identified as a potential UXO (assuming little error in the inversion process!);
- 2) Medium remanence, which we define as $m_t/3 < m_r < m_a$: In this case, the apparent remanence could vary from 0% ² to infinity! At worst the remanent magnetization would exactly cancel the induced magnetization producing a moment of 0. Depending on the orientation of the round and the remanence, shock demagnetization may or may not be required for these rounds to be classified as potential UXO.
- 3) High remanence: $m_r > 4 * m_a$: In this case, the remanence would never be smaller than about 75% ³. Therefore shock demagnetization would have to occur for the round to be classified as a potential UXO.

¹ Calculated assuming a worst case with the item perpendicular to the Earth's field and the remanence in the opposite sense to the inducted magnetization, so that $\%rem = m_r/3 / (m_r - m_t/3) = 50\%$.

² Where the remanence moves the moment from one point on the dipole feasibility curve to another point on the curve.

³ Calculated assuming a best case of remanence along the transverse axis with the remanence and induced magnetization aligned in the same direction.

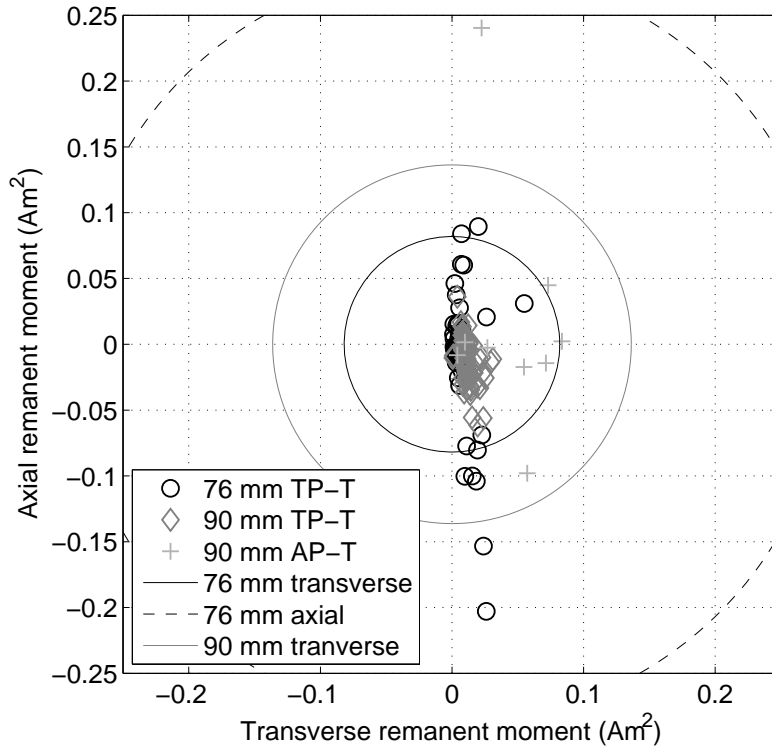


Figure 1. Remenant magnetization of 76 and two types of 90 mm projectiles measured with the MRIP platform at Limestone Hills, MT. Remanent magnetizations are split into the component along the axis of the project (axial) and across the axis (perpendicular). Contours delineating the values of the induced magnetizations of the 76 and 90 mm projectiles (as previously measured at the U.S. Army Corps of Engineers (USACE) Engineer Research and Development Center (ERDC) test stand) are also shown. The axial induced magnetization for the 90 mm projectile is larger than the range of values shown on the plot.

We measured all rounds soon after arrival at ATC and found that all except one were in the low-remenance category. Consequently, rounds were magnetized using the methodology described in Section 3.3. For the two higher remenance categories, we had two classes: one with the remanent magnetization predominantly along the traverse axis, and the other with the remanence predominantly along the axial axis (see Table 2). It turned out to be very difficult to magnetize items in the transverse direction and any attempts to generate items in the “high transverse” remanence category resulted in additional samples in the “medium transverse” or “high axial” categories. One of the high-axial remanence category items fired at maximum charge could not be recovered, thus there were only three items in that category instead of the intended four items.

Table 1. Test-matrix showing parameters that were varied. The numbers in brackets are the actual numbers achieved in each category.

Remanence	Low	Medium		High		Total
		Trans.	Axial	Trans.	Axial	
Projectile						
81 mm (minimum charge)	4 (5)	4 (6)	4 (4)	4 (0)	4 (6)	20 (21)
81 mm (medium-charge)	4 (9)	4 (5)	4 (4)	4 (0)	4 (5)	20 (23)
81 mm (maximum charge)	4 (5)	4 (8)	4 (4)	4 (0)	4 (3)	20 (20)

Table 2. Flight characteristics for the M879 mortars

Item	Charge	Firing Elevation		Muzzle Velocity mps	Range m	Time of Flight sec	Maximum Ordinate m	Angle of Fall (from horiz)		Impact Velocity	
		mils	deg					mils	deg	mps	mph
M879	0	983	55.3	66	400	11.3	147	999	56.2	64	143
M879	1	936	52.7	152	1900	23.9	672	1010	56.8	131	293
M879	4	1422	80.0	306	2000	52.2	3274	1468	82.6	219	490

3.3. Measurement procedure

The following measurement procedure was followed:

- 1) MRIP set-up: The MRIP platform was set-up close to the ATC demagnetization facility but at least 50 m from any power-lines and roads with passing traffic. Candidate areas were swept with Schonstedt magnetometers to ensure that the immediate area of the MRIP platform was free of large ferrous items.
- 2) Baseline survey of all rounds: All of the 81 mm mortars were measured on the MRIP platform (see section 3.3.2 for specific details) and sorted into low, medium and high remanence categories. Initially, all but one of the rounds was in a low-remanence category. During this process each round was assigned a unique label and a reference point was established on one side of the round. All magnetic measurements were subsequently oriented with the z-axis aligned with the long (axial) axis of the ordnance with positive pointing towards the ordnance nose, the y-axis transverse to the ordnance symmetry axis and pointing towards the reference marker, and the x-axis 90 degrees away and oriented to form a right-hand coordinate system.
- 3) Magnetization: Because all but one of the rounds were in a low-remanent state, the medium and high remanence rounds had to be obtained by magnetization of the rounds in non-destructive evaluation (NDE) equipment (see section 3.3.3 for specific details).
- 4) After magnetization in the chamber, the magnetic remanence of each round was measured on the MRIP, and additional magnetization was imposed if necessary.
- 5) Transportation of rounds and attachment of ignition cartridges: The rounds were then transported to a bunker close to the firing range and the ignition cartridges were attached.
- 6) Move MRIP and set-up adjacent to the firing range: The MRIP platform was moved closer to the firing range, in a location free of significant magnetic variation and at least 50 m from the nearest road and power-line. The selected location was close to the firing point so that rounds could be measured immediately before firing (see section 3.3.1 for details on the firing location).

- 7) Pre-firing measurement: A few hours before firing, the remanent magnetization of each round was again measured on the MRIP.
- 8) Firing of projectiles: Projectiles were then fired into the impact area. A number of spotting rounds were first fired to ensure that the test rounds would land within a specific area of I-field.
- 9) Impact location: Spotters in a control tower observed the ordnance impact and estimated a range and bearing to each target.
- 10) Relocation of rounds: The recovery team navigated to the approximate location of each round and placed a pin-flag at the entrance hole which was typically clearly visible. Some of the 0 charge increment rounds had their tails sticking out of the ground.
- 11) Excavation of rounds: For the shallower rounds (charges 0 and 1), shovels were used for excavation, while for the deeper rounds a combination of an excavator and a shovel was used. Every effort was made to ensure that each round did not suffer a significant shock during the excavation process. Because an excavator was used for the deeper charge 2 rounds, there is no guarantee that the rounds were extracted without being shocked.
- 12) Measurement of depth and orientation: The orientation and depth of each round that was excavated with a shovel was measured before removal. The measurements included the orientation of the z-axis of the ordnance item (in the direction of the reference point marked on each round). A photograph of each round was also taken.
- 13) Holding location: Each round was moved to a holding location adjacent to the MRIP.
- 14) Post impact measurement on MRIP: Each round was measured in the MRIP device which was relocated in the middle of I-field not far from the impact locations.

Additional details on the measurement procedures are provided in the field diary reproduced as Appendix A and the following three subsections.

3.3.1. Location of firing tests

The firing tests were conducted at I-field at the Aberdeen Proving Grounds (Figure 2). The charge 0 mortars were fired from a location immediately adjacent to the recovery field, whereas the charge 1 and 2 mortars were fired from a location about 500 m to the north-west. Spotters in a concrete bunker were used to visually estimate the location of round impact. This proved to be quite straightforward and all but one round were successfully recovered (the impact location of the missing round was located, but the round itself could not be found).

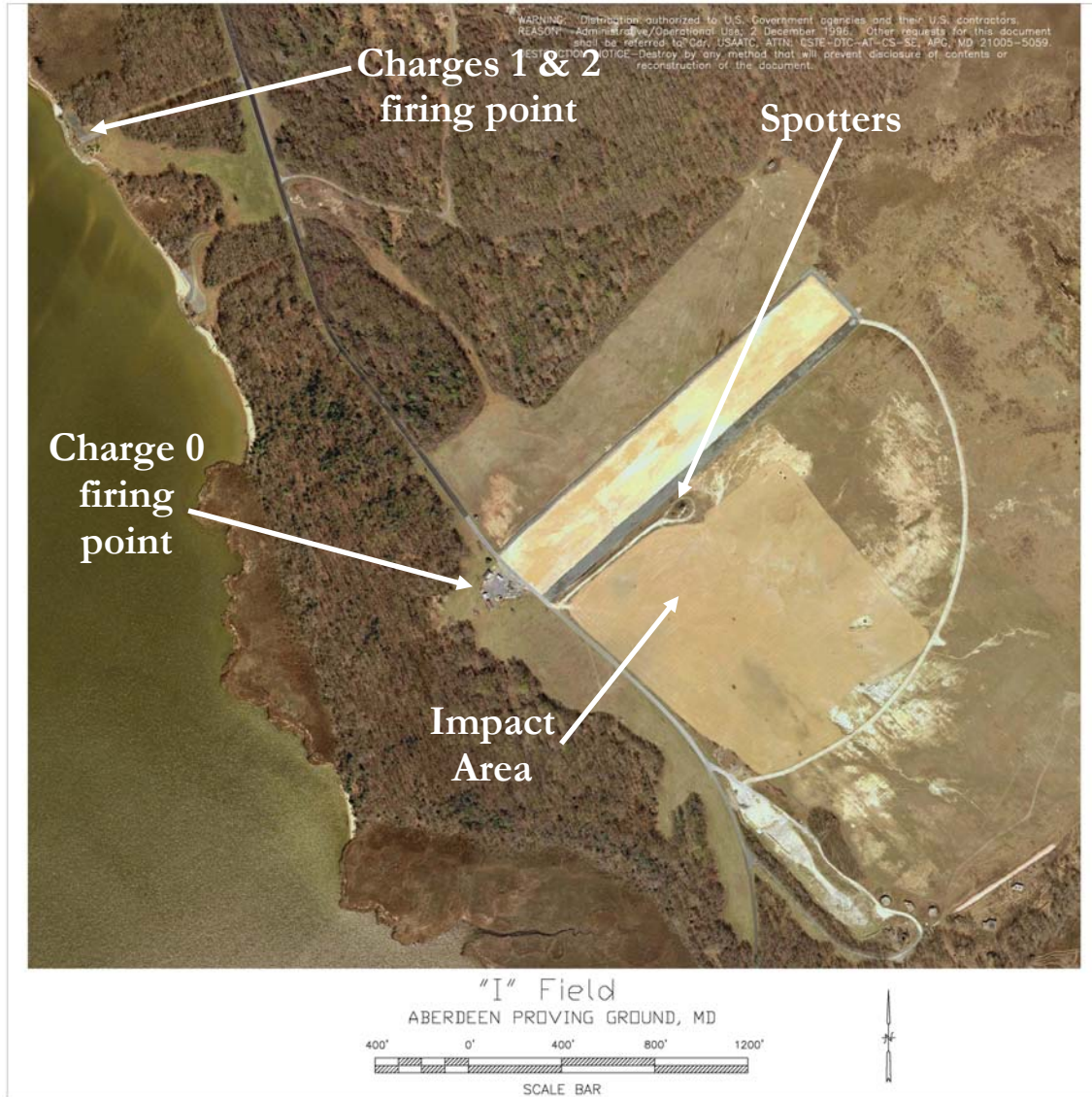


Figure 2. Location of the firing tests on the I-field site at Aberdeen Proving Ground.

3.3.2. MRIP measurement procedure

The following is a summary of the measurement procedure we used:

- 1) The MRIP was installed in a fixed location away from magnetic noise sources and buried ferrous objects or geology.
 - a. The sample table was oriented towards Magnetic North;
 - b. Each flux-gate magnetometer was rotated so that it reads 0, or near zero in the x-direction, and so that the y- and z-components are related by $B_z = -B_y \tan I$ (where I is the inclination of the Earth's field);
- 2) Calibration data was collected using a coil with known magnetic moment, that was successively oriented in three different directions;

- 3) Background measurements were collected before and after measuring each round so that diurnal variations could be removed from the sensor data.
- 4) Each item was carefully placed in the sample holder so that its reference frame was aligned accurately with the sensor's frame of reference (e.g., the y-axis of the sample is parallel to the y-axis of the sensor coordinate system).
- 5) Flux-gate magnetometer data were collected at a 12 Hertz (Hz) rate while the sample turntable was rotated through 360 degrees (at a rate of about 1 rotation every 30 seconds);
- 6) The sample was rotated by 90 degrees so that the top of the sample pointed East, and measurements were collected through another 360 degree rotation.
- 7) Using non-linear least squares, a model was fit to the two 360 rotations that comprises:
 - a. 3-components of remanent magnetization along the principal axes;
 - b. 3-components of induced magnetization along the principal axes;
 - c. The three Euler angles of the principal axes, relative to the sensor's frame of reference;
 - d. The two-components of the lever arm of the *center of magnetization* (apparent location of dipole moment) of the sample relative to the axis of the turntable, as well as the height of the center of magnetization above the turntable.
 - e. Quantities c) and d) were typically different for the two sets of rotation data due to differences in positioning and orientation of the samples.

3.3.3. Magnetization of rounds prior to firing

The behavior of ferromagnetic materials below the Curie temperature, under the influence of a magnetic field, is described by a hysteresis loop (Figure 3). Application of a magnetic field to a multi-domain grain causes preferential growth of domains with magnetization parallel to the field. If the applied field is strong enough, domain walls are destroyed and magnetization reaches saturation. On removal of the magnetizing field, domains reform and move back towards their initial position. Because of lattice imperfections and internal strains, domain walls settle in an energy minima that is different to their initial positions, and a small remanent magnetization results.

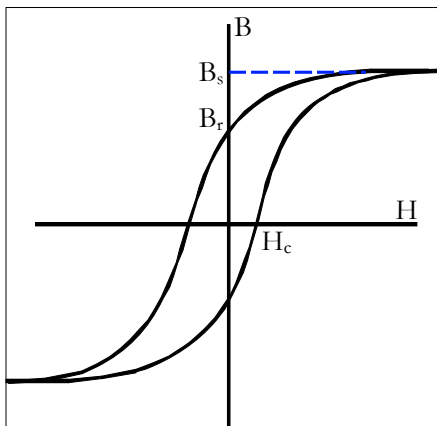


Figure 3. Example hysteresis curve.

To magnetize a steel sample, a H-6472 model direct current (DC)-magnetizer (Figure 4) was used. A large DC-magnetic field was applied to the sample and then the field was slowly reduced to 0. The active coil was 60 centimeters (cm) in diameter and 15 cm wide, with the usable field extending approximately 23 cm on either side of it. Thus an item up to 60 cm in length can be accommodated either axial or transverse to the coil axis. The amount of remanent magnetization was roughly checked using a Hall probe and confirmed by measuring the sample in the MRIP.



Figure 4. The Magnaflux A940 which is similar in appearance, although considerably smaller, than the Magnaflux H-6472 model we used (a photo was not available).

3.4. Results

The magnetic remanence as delivered, before firing and after impact of each round is listed in Table 3. As mentioned previously, only one round had significant remanent magnetization when delivered (item 58 with a remanent magnetization of 0.118 Am^2). Therefore the medium and high remanence category rounds had to be obtained by magnetization of the rounds in the Magnaflux H-6472. It was not possible to impose a strong magnetization in the transverse direction. Hence no rounds were generated in the “high transverse” category: instead extra samples in the “medium transverse” and “high axial” categories were generated. An additional five mortars (numbers 61 to 65) were made available just before firing and these contributed an extra five “low remanence” category items to the test-matrix. One of the mortars fired with 2 charge increments (number 33) was not recovered.

Orientations and depths of recovered rounds are shown in Table 4. All the mortars fired with two charge increments, and several of the mortars fired with one charge increment, penetrated the ground by more than 60 cm (2 feet) and had to be extracted with the help of an excavator. Orientation and depth measurements could not be made on any of the excavator extracted mortars.

In Figure 5 we plot the axial and transverse remanent magnetization before and after firing and impact for charges 0, 1 and 2. A grey line joins the measurements for a given round. Also shown on the plot are the transverse and axial induced magnetizations for the 81 mm rounds. These provide an indication of the magnitude of the remanent magnetization compared to the possible range of induced magnetizations (any value between the transverse and axial magnetizations). Several observations can be made from the plots:

- (1) As the number of charge increments increases a larger proportion of the before firing remanent magnetization is lost after impact. This confirms the shock demagnetization occurs and demonstrates that the degree of demagnetization is dependant on the shock of impact (as intuitively expected).
- (2) The rounds with low initial remanent magnetization actually increase their remanence after impact. This confirms that shock magnetization occurs (where the round acquires a component of remanent magnetization in the direction of the ambient field at the time of impact).

Table 3. Magnetic remanence of rounds as delivered, before firing and after impact.

Label	Original remanence				Remanence before firing				Remanence after impact			
	x-Am ²	y-Am ²	z-Am ²	T-Am ²	x-Am ²	y-Am ²	z-Am ²	T-Am ²	x-Am ²	y-Am ²	z-Am ²	T-Am ²
Charge 0												
1	0.005	0.008	0.004	0.010	0.007	0.010	0.004	0.013	-0.006	0.073	-0.004	0.073
2	0.007	0.015	0.000	0.016	0.004	0.017	0.000	0.017	-0.001	0.081	-0.002	0.081
3	0.006	0.003	0.003	0.008	0.006	0.006	0.002	0.008	-0.006	0.095	-0.003	0.095
4	0.005	0.007	0.005	0.010	0.004	0.007	0.004	0.009	-0.006	0.102	-0.007	0.102
5	0.004	0.002	0.010	0.010	-0.008	0.215	-0.006	0.216	-0.018	0.179	-0.020	0.181
6	0.000	0.005	0.010	0.011	0.006	-0.230	0.020	0.230	0.005	0.031	0.004	0.031
7	0.005	0.003	0.000	0.005	0.012	-0.160	0.017	0.161	0.004	0.012	0.005	0.013
8	0.003	0.014	0.007	0.016	-0.013	0.266	-0.015	0.267	-0.017	0.165	-0.020	0.167
9	0.009	0.000	0.003	0.009	0.118	-0.001	0.050	0.128	0.046	0.044	0.021	0.067
10	0.009	0.003	0.003	0.010	-0.096	0.526	-0.052	0.537	-0.052	0.196	-0.027	0.204
11	0.005	0.000	0.007	0.009	-0.151	0.051	-0.002	0.159	-0.087	0.108	0.003	0.139
12	0.007	0.006	0.007	0.012	0.062	1.098	-0.084	1.103	-0.040	0.457	-0.101	0.470
13	0.006	0.005	0.000	0.008	0.020	-0.666	0.032	0.667	0.047	-0.422	0.049	0.427
14	0.008	0.011	0.005	0.015	0.095	-0.936	0.016	0.940	0.057	-0.397	0.036	0.402
15	0.005	-0.012	0.003	0.013	-0.091	1.072	-0.083	1.079	-0.073	0.571	-0.070	0.580
16	0.004	0.008	0.004	0.010	0.036	-0.774	0.032	0.775	0.052	-0.431	0.058	0.438
17	0.004	0.000	0.004	0.005	-0.122	-0.144	0.077	0.203	-0.052	-0.064	0.027	0.087
18	0.003	0.005	0.002	0.006	-0.025	0.034	0.123	0.130	-0.022	0.073	0.043	0.088
19	0.005	0.006	0.005	0.009	0.050	0.070	0.129	0.155	0.015	0.017	0.040	0.046
20	0.004	-0.008	0.007	0.011	-0.092	-0.005	-0.109	0.143	-0.059	0.112	-0.071	0.145
21	0.006	0.008	0.002	0.010	0.005	0.008	0.003	0.010	-0.007	0.093	-0.005	0.093
Charge 2												
22	0.008	0.005	0.003	0.010	0.007	0.009	0.002	0.012	-0.001	0.053	0.001	0.053
23	0.009	0.009	0.004	0.013	0.005	0.005	0.000	0.007	0.009	-0.004	0.011	0.015
24	0.008	0.010	0.010	0.016	0.003	0.009	0.004	0.010	0.009	0.025	0.006	0.027
25	0.004	0.007	0.003	0.008	0.010	-0.075	0.012	0.076	0.000	0.021	0.004	0.021
26	0.007	0.008	0.002	0.011	0.005	-0.170	0.020	0.171	0.002	0.063	-0.002	0.063
27	0.007	-0.001	0.004	0.008	0.013	-0.305	0.022	0.306	0.004	-0.012	0.006	0.014
28	0.002	0.016	0.004	0.017	0.001	0.240	0.003	0.240	0.003	0.013	0.005	0.014
29	0.007	-0.002	0.005	0.009	-0.131	0.053	-0.040	0.147	-0.017	0.015	0.004	0.023
30	0.009	0.015	0.007	0.019	0.091	0.034	0.041	0.106	0.010	0.134	0.009	0.135
31	0.007	0.014	0.006	0.016	-0.091	0.050	0.000	0.104	-0.012	0.036	-0.003	0.038
32	0.003	0.002	0.011	0.011	-0.042	-0.163	-0.153	0.227	-0.015	-0.005	-0.020	0.025
33	0.003	0.014	0.007	0.016	-0.049	0.857	-0.036	0.859				
34	0.003	0.005	0.006	0.008	0.009	-0.994	0.037	0.995	0.008	-0.132	0.019	0.133
35	0.007	0.004	0.007	0.010	0.077	-1.026	0.074	1.032	0.028	-0.290	0.037	0.293
36	0.005	0.009	0.003	0.011	-0.031	0.799	-0.025	0.800	-0.016	0.180	-0.020	0.181
37	0.013	0.007	0.009	0.017	0.036	-0.064	0.142	0.159	0.015	-0.016	0.026	0.034
38	0.009	0.005	0.006	0.012	0.054	-0.075	0.150	0.176	0.016	0.017	0.024	0.033
39	0.010	0.008	0.004	0.013	0.057	-0.092	0.127	0.167	0.019	0.003	0.017	0.025
40	0.006	0.017	0.007	0.019	0.091	-0.119	0.139	0.204	0.020	0.000	0.024	0.031
41	0.006	0.008	0.002	0.010	0.006	0.002	0.005	0.008	0.004	0.012	0.003	0.013
42	0.001	-0.001	0.002	0.002	0.003	-0.001	0.005	0.006	0.001	0.043	0.010	0.045

Label	Original remanence				Remanence before firing				Remanence after impact			
	x-Am ²	y-Am ²	z-Am ²	T-Am ²	x-Am ²	y-Am ²	z-Am ²	T-Am ²	x-Am ²	y-Am ²	z-Am ²	T-Am ²
Charge 1												
43	0.009	0.005	0.005	0.012	0.011	0.004	0.006	0.013	0.000	0.070	-0.003	0.070
44	0.005	0.002	0.006	0.008	0.007	0.005	0.008	0.012	0.002	0.052	-0.001	0.052
45	0.004	0.008	0.008	0.012	0.010	-0.201	0.018	0.202	0.013	-0.023	0.007	0.027
46	0.007	0.000	0.005	0.008	0.000	0.211	-0.001	0.211	0.007	0.042	0.003	0.042
47	0.008	-0.004	0.011	0.014	0.017	-0.186	0.024	0.188	0.006	-0.006	0.002	0.008
48	0.003	-0.002	0.007	0.008	0.010	-0.029	0.009	0.032	0.002	0.032	-0.002	0.032
49	0.008	0.005	0.010	0.013	-0.012	0.408	-0.135	0.429	-0.012	0.068	-0.034	0.077
50	0.011	0.012	0.004	0.016	0.007	0.008	0.003	0.011	-0.001	0.065	-0.004	0.065
51	0.005	0.010	0.009	0.015	0.000	0.006	0.009	0.010	0.000	0.072	-0.004	0.072
52	0.005	0.005	0.008	0.011	-0.002	0.403	-0.104	0.416	-0.012	0.074	-0.030	0.081
53	0.006	0.011	0.008	0.015	0.122	0.399	-0.086	0.426	0.015	0.115	-0.030	0.120
54	0.007	0.009	0.007	0.013	0.002	-0.009	-0.115	0.115	0.002	-0.103	-0.022	0.106
55	0.003	0.006	-0.001	0.007	-0.030	0.766	-0.019	0.766	-0.034	0.254	-0.025	0.258
56	0.011	0.002	0.005	0.012	-0.061	1.032	-0.066	1.036	-0.042	0.352	-0.039	0.357
57	0.003	0.021	0.002	0.021	0.103	-0.090	0.112	0.177	0.012	0.018	0.035	0.041
58	0.003	0.117	0.010	0.118	0.150	-0.087	0.191	0.258	0.040	0.096	0.054	0.117
59	0.006	0.011	0.010	0.016	0.040	-0.067	0.134	0.155	0.008	0.024	0.035	0.043
60	0.005	0.012	0.008	0.015	0.084	-0.117	0.116	0.185	0.022	0.011	0.026	0.036
61					0.007	0.010	-0.001	0.012	-0.001	0.043	-0.004	0.043
62					0.005	0.002	0.003	0.006	0.001	0.013	0.005	0.014
63					0.003	0.019	0.004	0.019	-0.002	0.063	-0.002	0.063
64					0.006	0.009	0.007	0.012	0.003	0.042	0.002	0.042
65					0.004	0.004	-0.001	0.006	-0.002	0.040	-0.001	0.040

The second observation regarding shock magnetization is more readily apparent in the zoomed-in views shown in Figure 6. Close-inspection of this plot reveals that the amount of shock magnetization decreases with increasing number of charge increments. Also shown on the plots is a contour which delineates the regime where the apparent remanence would always be less than 50% regardless of the final orientation of the projectile. If all projectiles were within this regime, discrimination using the apparent remanence metric would be a viable and (potentially) reliable method for UXO discrimination. For each of the charge increments, there are a number of cases where the after impact remanence places the item outside this regime: hence discrimination using remanence would not be reliable. A second contour delineates the regime where all possible orientations would produce an apparent remanence of less than 75%. There are still a number of after impact remanence values that lie outside this regime, with the number decreasing with increase in charge increment. Thus apparent remanence discrimination becomes more reliable the larger the shock of impact, but even at high shocks, rounds with large preexisting remanence may not be demagnetized sufficiently for reliable discrimination.

Table 4. Orientations and depths of recovered items.

Label	Hole orien.	Round orien.	Notch Orien.	Dip of round	Depth (cm)	Charge	Comment	Excav. used?
1	125	125	114	5	26	0	Buried	
2	167	167	298	23	-4	0	Measurement of notch orientation could be suspect as pulled this one out before the notch was found	
3	176	176	5	1	-7	0		
4	180	180	0	24	NaN	0	Buried in gully,	
5	115	115	40	19	0	0		
6	157	157	190	19	-1.5	0		
7	155	155	135	19	15	0	Buried	
8	140	140	280	18	35	0	Buried, orientation measurement susept	
9	110	110	300	15	33	0	Buried	
10	133	133	140	NaN	0	0	On edge of gully	
11	156	156	270	15	8	0	Buried	
12	150	150	150	27	1	0		
13	220	220	38	29	-23	0	On gully edge, hit side of gully (glancing blow) and didn't penetrate far	
14	140	140	240	36	0	0		
15	144	144	185	30	-2.5	0	Buried	
16	147	147	290	22.5	-0.5	0		
17	172	172	210	15	-5.5	0		
18	152	152	178	24	13.5	0		
19	134	134	290	33	1	0		
20	125	125	85	16	0	0	Tail sticking out on edge of gully	
21	195	195	80	24	0	0	Tail sticking out on edge of gully	
22						2	No fuze	Yes
23						2		Yes
24						2		Yes
25						2		Yes
26	175					2		Yes
27	175					2		Yes
28	180					2		Yes
29						2		Yes
30						2	No fuze	Yes
31						2	No fuze	Yes
32						2	No fuze	Yes
33						2	Round missing	Yes
34						2	No fuze	Yes
35						2	No fuze	Yes
36	180					2		Yes
37						2	No fuze	Yes
38	155					2		Yes
39	195					2		Yes
40						2	No fuze	Yes
41						2		Yes
42	174					2		Yes

Label	Hole orien.	Round orien.	Notch Orien.	Dip of round	Depth (cm)	Charge	Comment	Excav. used?
43		156	109	21	59	1		Yes
44	150	160	267	17	47	1		
45	166	157	180	29	46	1		Yes
46	156	168	27	25	51	1		Yes
47		150	18	25	48	1		Yes
48	145					1	Couldn't locate this round using a shovel	Yes
49		150	322	23	54	1		
50		133	160	8	42	1		
51	160	165	75	24	62	1		Yes
52	161	172	92	18	50	1		
53	145	147	205	28	66	1		
54	148	145	2	35	62	1		Yes
55	140	166	200	29	42	1		
56		175	95	23.5	49	1		
57	145	155	82	21	50	1		
58	165					1	Couldn't locate this round using a shovel	Yes
59						1	Couldn't locate this round using a shovel	Yes
60	150	155	350	32	48	1		
61	160	155	155	30	56	1	Notch was hard to find, may not be correct	
62		162	92	36	53	1		Yes
63	155	138	88	24	54	1		
64	177					1		Yes
65	165					1		Yes

Close inspection of the axial and transverse remanent magnetizations of the mortars fired with no charge increment in Figure 5a reveals a tendency of some of the high remanence rounds to acquire more transverse remanence after impact than they possessed before firing. Figure 7 provides an alternative visualization of the change in remanence between the before firing and after impact scenarios that provides an explanation for this observation. The remanence is split into components parallel and perpendicular to the inducing field at the time of impact. We assume that the final orientation of the round is the same as the orientation at the time of impact and use the MRIP measured transverse and axial induced magnetizations to estimate the direction of the inducing field within the mortar. We can only show results for mortars fired with 0 and 1 charge increments as orientation measurements were not made on the mortars fired with two charge increments. Almost all the mortars, fired with both charge increments, appear to be moving towards a final state with a modest amount of magnetization in the ambient field direction, with zero magnetization in the direction perpendicular to the ambient field. This progression results in the increase in the remanent magnetization evident in the transverse component of magnetization of several of the measurements shown in Figure 5a (the shock magnetization phenomenon).

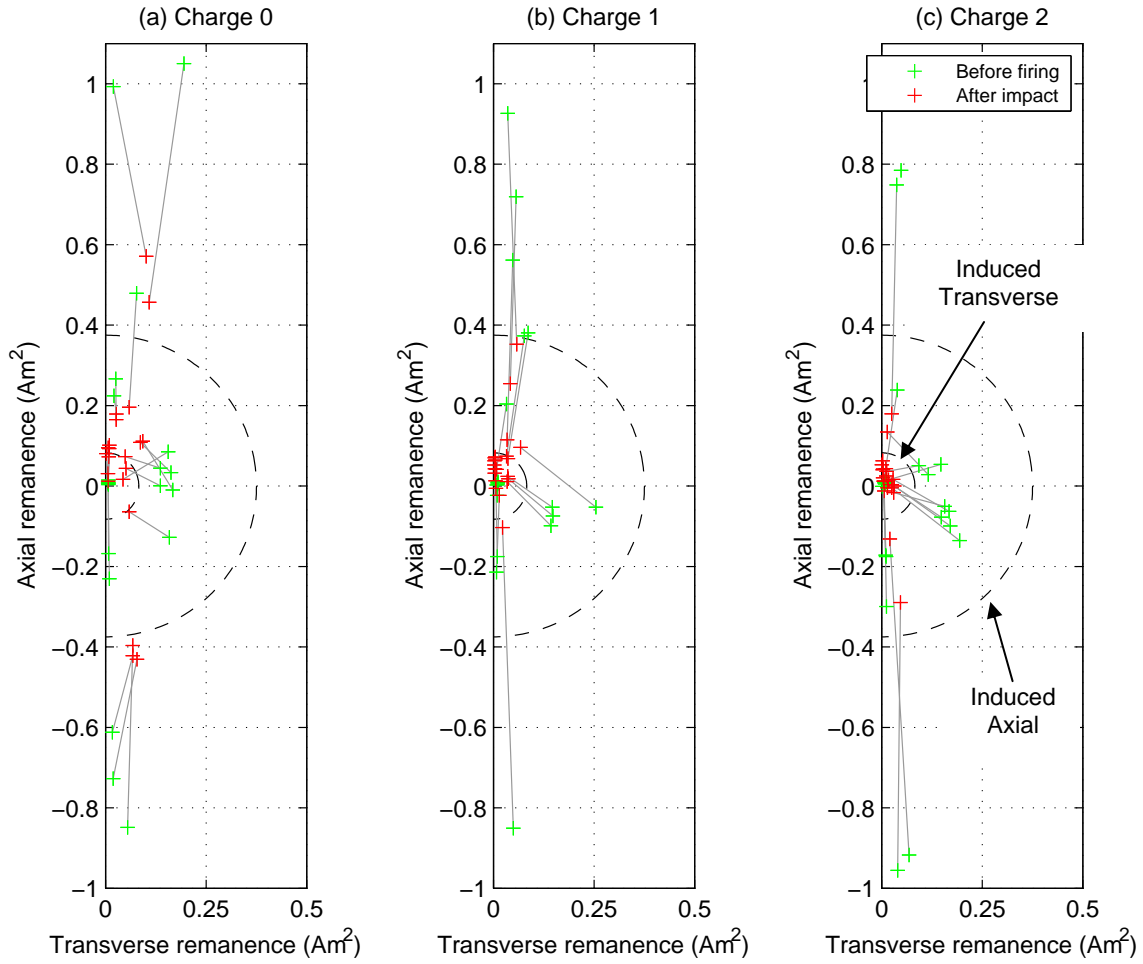


Figure 5. Change in remanence after firing and impact for (a) charge 0; (b) charge 1; and (c) charge 2. The two dashed black circles delineate the transverse and axial induced magnetizations for the 81 mm mortar. A grey line joins the before firing and after impact values for a given item.

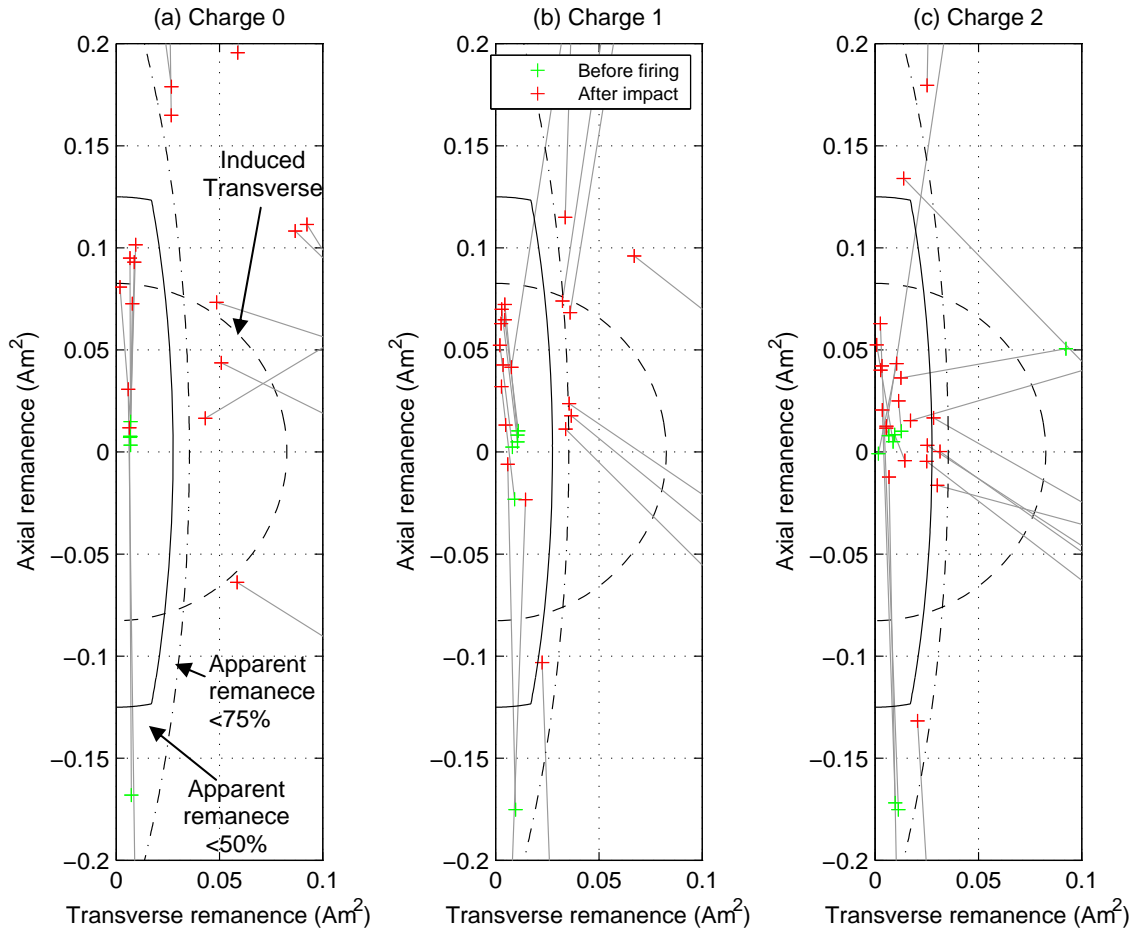


Figure 6. Zoomed in view of the change in remanence after firing and impact for (a) charge 0; (b) charge 1; and (c) charge 2. A grey line joins the before firing and after impact values for a given item. Also shown on this plot are contour that delineate the regimes where apparent remanence is always less than 50% and 75%.

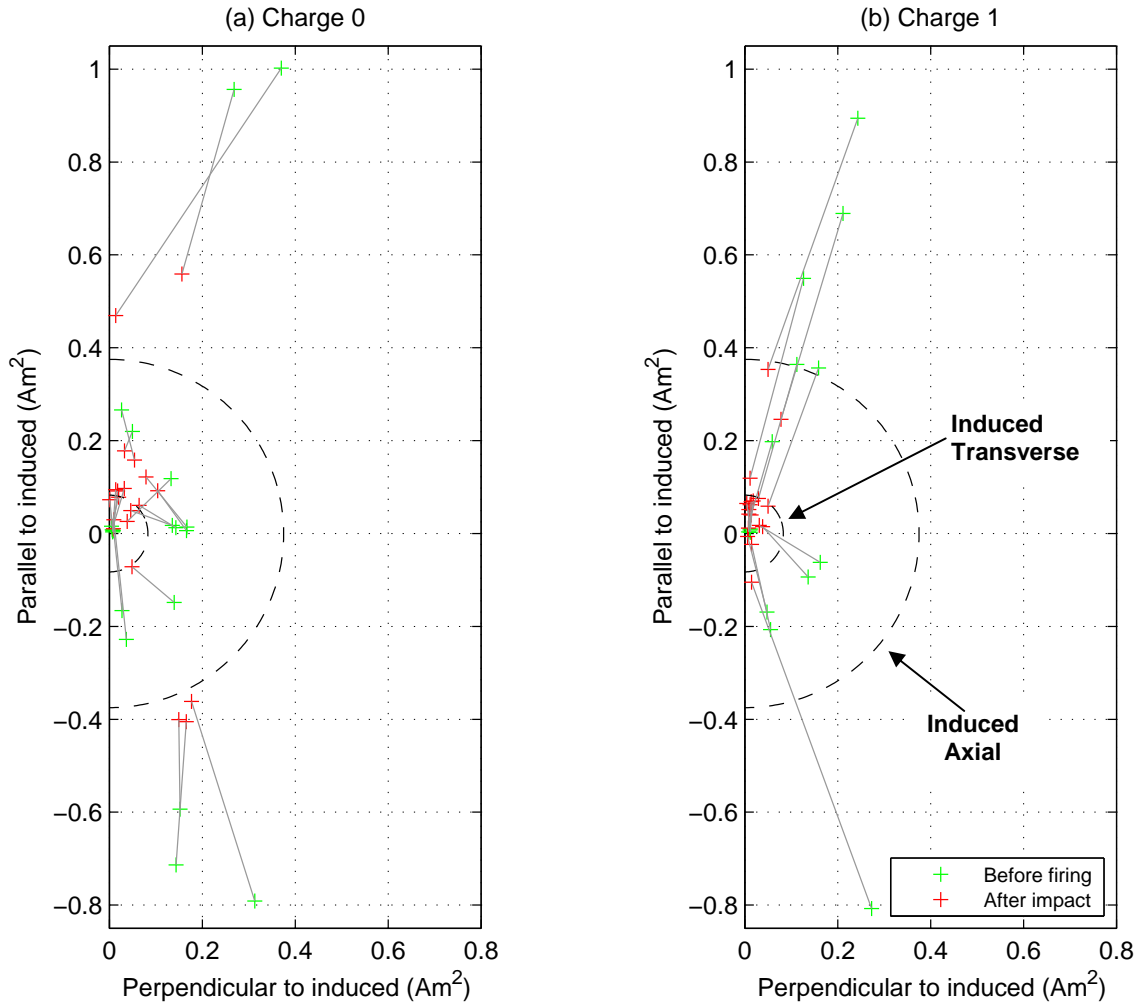


Figure 7. Change in remanence after firing and impact for (a) charge 0; and (b) charge 1, with remanent moments split into components parallel and perpendicular to the induced field at the time of impact. A grey line joins the before firing and after impact measurements for a given item.

Next, we take a closer look at the distribution of the apparent remanence values for the low, medium and high initial remanence samples both before firing and after impact (Figure 8). To calculate these cumulative distributions we generated 5000 random orientations of each item, and computed the apparent remanence that resulted when the induced and remanent magnetizations were added together. We then combined the apparent remanence distributions for each item within a given class (e.g low initial remanence, before firing, charge increment 0 constitutes one class) to come up with one cumulative distribution per class. Considering the low initial remanence category first (first row of Figure 8), we see that the apparent remanence is **larger** after impact than it was before firing. In addition, the change in apparent remanence is greatest for the mortars fired with 0 charge increment. This result reflects our earlier observation that shock magnetization decreases with increasing charge increment. Turning now to the medium and high initial remanence categories (second and third rows of Figure 8) we see that the apparent remanence tends to decrease after impact, with a greater change with increasing charge increment. For medium initial remanence, charge increments 1 and 2 are sufficient to reduce the apparent remanence to less than 50% for virtually all possible

orientations. For high initial remanence, there are still significant numbers (40 and 25% for charge increments 1 and 2) of orientations with apparent remanence greater than 50%.

The results presented in the previous paragraph concern the distribution of apparent remanence for any arbitrary final orientation of the mortar. As such they could be overly pessimistic as the final remanence magnetization is influenced by the ambient magnetic field at the time of impact. That is, there is some relationship between the induced magnetization and the after impact remanent magnetization. Figure 9 plots the apparent remanence in the as-found orientation of each round for the before firing and after impact remanent magnetizations. We can only show the results for the mortars fired with 0 and 1 charge increment as no orientation measurements were made on the mortars fired with two charge increments. Similar to the results in the previous paragraph there is an increase in apparent remanence for the mortars that initially had low remanent magnetization, and a decrease in apparent remanence for mortars with medium and higher initial remanent magnetization.

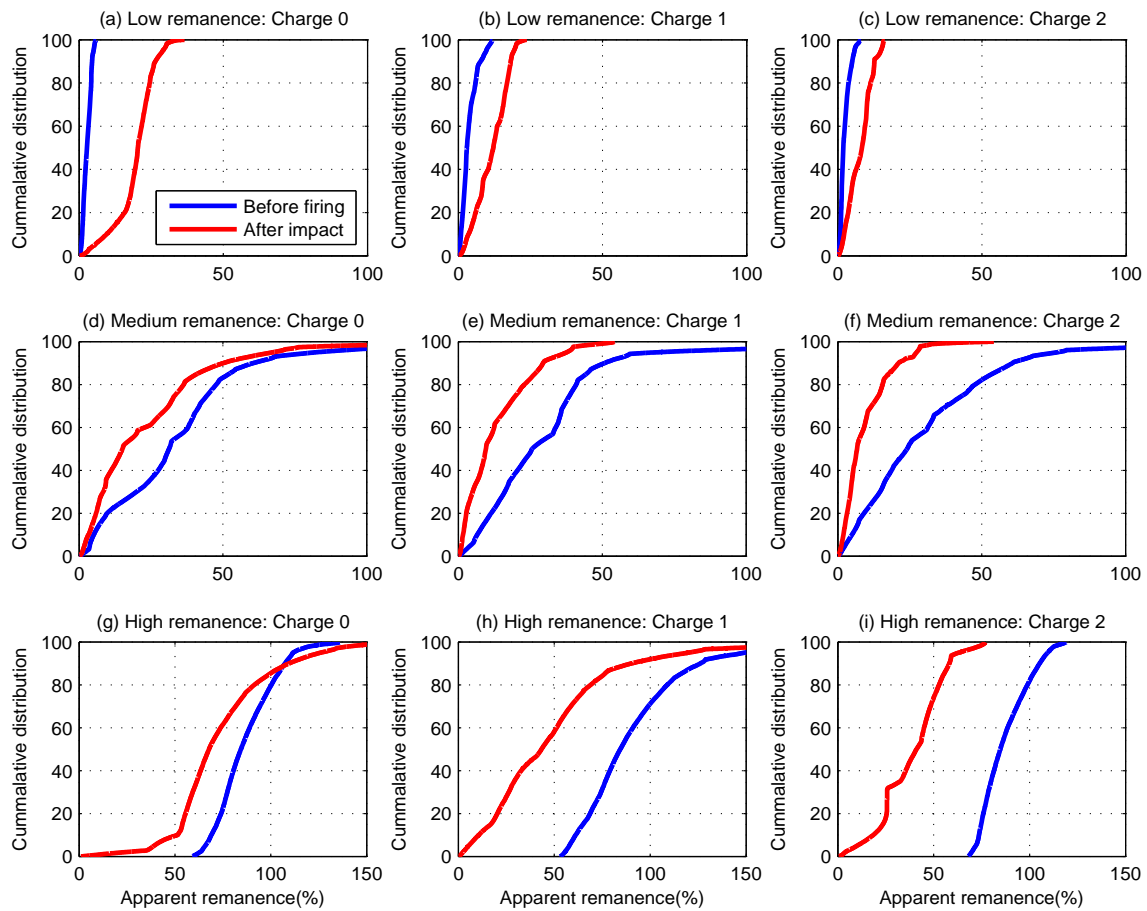


Figure 8. Cumulative histograms of apparent remanence for rounds before and after firing. The results are presented separately for the different charge increments (as columns) and for difference amounts of initial remanence (low, medium and high are top, middle and bottom rows respectively).

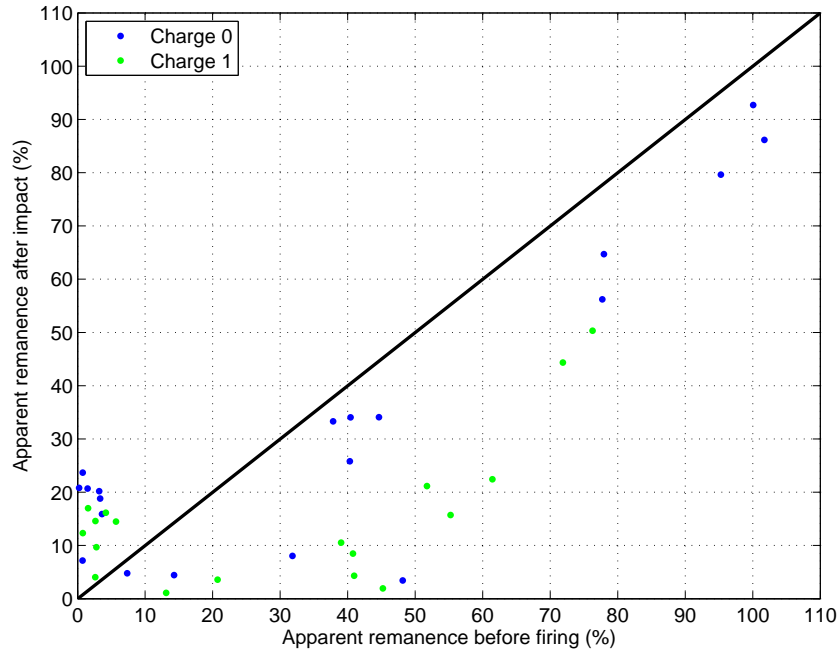


Figure 9. Apparent remanence in the ‘as found’ orientation for before firing and after impact.

We next present a simple model that approximates the change in magnetization observed in the mortars fired at the three different charge increments. The model is linear and comprises a percentage change in magnetization and an offset value. The offset value accounts for the observation that the mortars are not progressing to a state of zero remanence, but instead appear to be acquiring a remanence in the direction of the ambient field. Linear models were generated for axial and transverse remanence and for remanence parallel and perpendicular to the ambient field at the time of impact (no results are provided for these last two for the mortars fired with 2 charge increments). The modelling results are shown in Figure 10 with model coefficients listed in Table 5. For the mortars fired with 0 charge increment, just over 50% of the initial magnetization in the axial or ambient field directions remains after impact, compared to 23% left for 1 charge increment. The percentage change in axial remanence of the mortars fired with 2 charge increments is similar, but the offset value is smaller (that is, the amount of magnetization acquired in the direction of the ambient field is decreased). Larger decreases in magnetization in the transverse and perpendicular to ambient field directions occur for all charge increments.

Table 5. Parameters of the linear models in Figure 10.

	Charge 0		Charge 1		Charge 2	
	Offset	%change	Offset	%change	Offset	%change
Axial remanence	0.0401	51	0.0466	23	0.0281	22
Transverse remanence	0.0249	31	0.0104	22	0.009	10
Parallel with induced	0.0471	52	0.0421	24	NA	NA
Perpendicular to induced	0.0256	31	0.0088	15	NA	NA

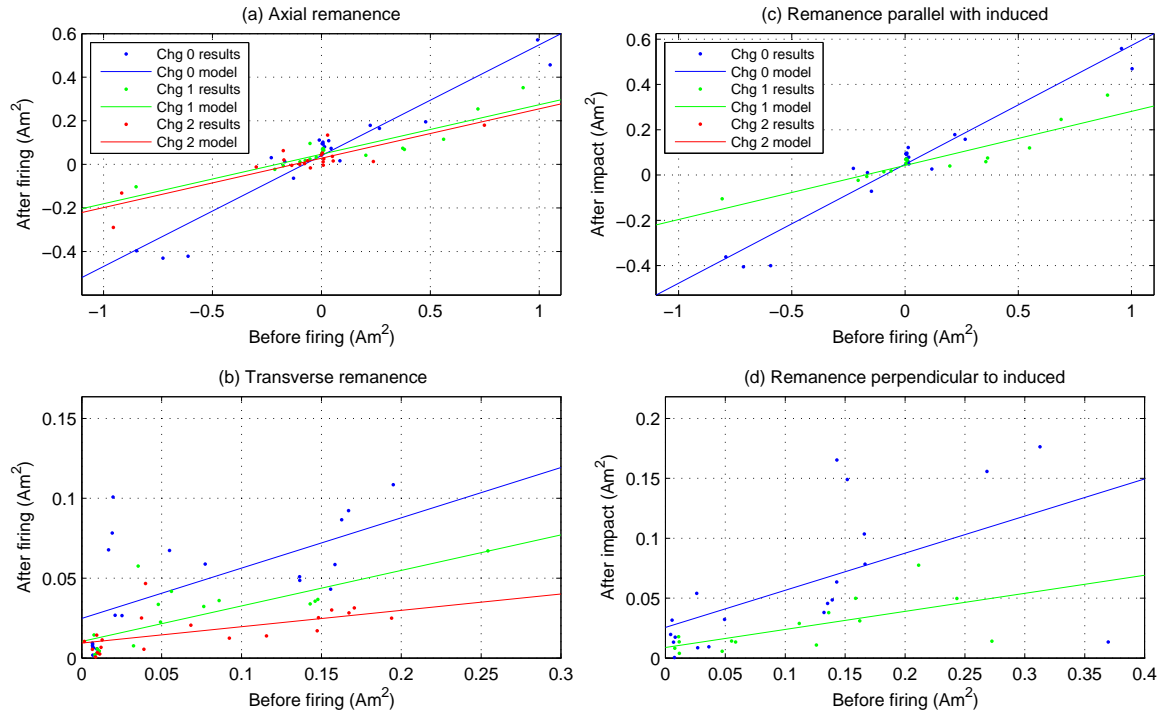


Figure 10. Linear model of the change in remanence for the mortars fired at different charge increments: (a) compares axial remanence; (b) compares transverse remanence, while (c) compares the magnetization in the direction of the induced magnetization at the time of impact (charge 2 results not shown as no orientation measurements were made), with (d) the results for the remanence perpendicular to the inducing field.

3.5. Discussion and Conclusions

The ATC firing tests were intended to answer the following open questions (conclusions from this study are listed following each question):

- 1) To what extent does shock demagnetization erase the remanent magnetization of ordnance?
 - a. Shock demagnetization occurs and resulted in projectiles with significant remanence losing between 50 and 70% of their initial magnetic remanence.
- 2) Do ordnance acquire a shock remanent magnetization when they impact the ground?
 - a. Yes, projectiles do acquire a remanent magnetization in the direction of the ambient field at the time of impact. The amount of this acquired remanence appears to decrease with increasing impact shock.
- 3) How does impact velocity affect the amount of shock demagnetization that occurs?
 - a. At the lowest impact velocity considered (64 m/s) remanent magnetization decreased by about 50% compared to a 70% decrease at the highest impact velocity (210 m/s). The lower impact velocity rounds also acquired a larger magnetization in the direction of the inducing field at the time of impact ($\sim 0.047 \text{ Am}^2$ compared to 0.028 Am^2).
- 4) Will rounds with extremely large remanent magnetization undergo sufficient shock demagnetization to be correctly classified using the apparent remanence method?
 - a. For this type of soil and projectile, shock demagnetization is insufficient to erase the remanent magnetization of the highly magnetized rounds at the highest impact velocity achieved (210 m/s).

Additional discussion of the results is left to the summary and conclusions section of this final report.

4. Measurement of the Remanent Properties of UXO and Shrapnel in the Field (Task 3)

We deployed the MRIP to two field sites, Limestone Hills Montana and Camp Sibert Alabama. The results are presented in the paper, Billings (2009). The abstract for this publication appears in Section 2.0.

5. Development of a theoretical or empirical model of shock induced changes to magnetization (Task 4)

Efforts to develop a model of shock induced changes to magnetization are summarized in Appendix B.

6. Collection of test-stand data over munitions (Task 5)

This task was completed in 2005 and a paper was published in IEEE Transactions on Geoscience and Remote Sensing, Billings et al. (2006). The abstract from this publication follows:

“Magnetometry is widely used for the characterization of areas contaminated by unexploded ordnance (UXO). To successfully discriminate hazardous UXO from nonhazardous clutter requires accurate models of the ordnance response. This paper develops an ordnance library with 15 different items using total-field magnetic data collected over a test stand. The induced and remanent magnetizations were obtained by varying the three-dimensional orientation of each item and measuring the magnetic field on a horizontal plane in the dipolar regime. Replicate measurements using multiple specimens of the same ordnance returned very similar induced magnetizations. The fitted moments were used to estimate the detection depths for different sensor noise floors. A prolate spheroid with a 3.5 aspect ratio was used to provide a good approximation to the detection depths for many of the ordnance items. Assuming a 1-nT noise floor, these orientation-dependent detection depths ranged from 10 to 17 times of the object's diameter.”

7. Incorporation of magnetic discrimination methods into a workable software system (Task 6)

This task was completed, and the remanence discrimination method is available in the UXOLab software environment. The method has been applied in a production setting at Chevallier Ranch and Limestone Hills, MT (see Billings and Youmans, 2007) and at the Former Camp Sibert (see Billings et al., 2008). The abstracts for these publications follow.

Billings & Youmans, 2007 *“Advanced discrimination methods and careful optimization of operational procedures are critical for efficient remediation of unexploded ordnance (UXO) contaminated sites. In this paper, we report on our experiences with a 200 acre magnetic survey that was collected and processed under production survey conditions at Chevallier Ranch, Montana. All anomalies with fitted moments above 0.05 Am² were excavated. During the survey the magnetic remanence metric was predicted but not used to guide the discrimination. The retrospective analysis presented here reveals that discrimination using remanence would have significantly reduced the total number of*

anomalies (with good dipolar fits) that needed to be excavated, from 524 to 290 while still recovering all 69 UXO. The false alarm rate (FAR = number of non-UXOs excavated divided / number of UXO found) was reduced from 6.3 to 2.9. At a cut-off of 75% remanence, 77% of anomalies due to shrapnel and metallic debris and 64% of geological anomalies were rejected.

Geological anomalies due to variations in magnetite concentration introduced a significant human-element into the interpretation process. Three different interpreters added a total of 305 additional anomalies that were not fit with a dipole model and which were later found to be non-UXO. Between 40 and 50% of anomalies picked by the two relatively inexperienced interpreters who analyzed the data turned out to be geology, as compared to 14% for an experienced interpreter. Critical analysis of results, operator training and feedback from the UXO technicians validating the anomaly are essential components towards improving the quality and consistency of the anomaly interpretations. This is consistent with the tenants of Total Quality Management (TQM). We compare the actual FAR that resulted during the survey when there was little feedback between UXO technician validation results, to a hypothetical result that could have been achieved had there been a constant feedback system in place at the onset of operations. Feedback would have significantly reduced the number of geological anomalies and decreased the FAR from 10.7 to 4.0.

The hypothetical results presented here demonstrate the value of using TQM principles to guide the UXO remediation process. They further show that improvements in the efficiency and costs of UXO remediation require both technological advances and operational optimization of the technology when implemented in a production setting. Furthermore, by treating geophysical modeling and UXO validation as separate entities, both with respect to contracting and operational reporting, there is little incentive for the geophysicist to leave an anomaly off the dig-sheet. Only potential negative consequences will result if that anomaly is later found to be a UXO. An incentive based mechanism that rewards the geophysicist for reductions in follow-on costs would have a strong potential to reduce the number of unnecessary excavations, and hence reduce the total cost of the UXO remediation effort.”

8. Measurement of Viscous Remanent Magnetization at the Institute for Rock Magnetism (Task 7)

During the project, two visits were made to the Institute for Rock Magnetism for the purpose of measuring the magnetic properties (in particular the magnetic viscosity) of a number of steel samples. Specific objectives were to:

- (i.) Determine the importance of magnetic viscosity to measurements made by MRIP (time scale from 1 to 100 seconds);
- (ii.) Determine the impact of magnetic viscosity on the long-term remanence of unexploded ordnance (time-scales of days to tens of years); and
- (iii.) Characterize the remanence and coercivity of the steel used in projectiles.

Fresh steel, unfired projectiles, unexploded ordnance, and shrapnel samples were prepared for measurements of magnetic viscosity. The M353 90 mm target practice round is made of forged, hot rolled AISI 1010 low carbon steel (Defense Ammunition Center, 2006). A hot rolled carbon steel, grade 1010, bar was thus obtained and three samples cut from the bar (Figures 11 and 12).

All samples in this study were cut with a hacksaw using a bi-metal blade, and consequently polished on all cut sides with three grades of diamond hone to remove any metal pieces which may have broken off of the blade and become lodged in the sample.

Larry Overbay, of ATC provided half of the main shell body of both an 81 mm M821/M889 mortar high explosive (HE) and a 120 mm M1 HE unfired projectile (Figures 13 and 14).



Figure 11. Low carbon steel bar from which samples were obtained.



Figure 12. Samples cut from low carbon steel bar.



Figure 13. Unfired 81 mm M821/M889 mortar HE.



Figure 14. Unfired 120 mm M1 HE



Figure 15. Sample from unfired 81 mm M821/M889 mortar HE.



Figure 16. Samples from Unfired 120 mm M1 HE.

The 81 mm is comprised of forged steel alloy (HF-1). The 120 mm round is forged low carbon steel AISI 1008 (MPT ARDEC, 2005). Three samples were taken from the top and center of each of these round halves (Figures 15 and 16). The sides of the round halves were specifically avoided during sampling, as the halving of these rounds may have heated up their edges possibly changing the magnetic properties.

Clif Youmans of the Montana Army National Guard provided a 90 mm M353 target practice round, and an 81 mm mortar from Limestone Hills Training Area, near Townsend, Broadwater County, Montana. Samples were cut from the top center of each of these rounds (Figures 17 to 20). In addition Youmans provided several shrapnel samples also taken from Limestone Hills (Figure 21).



Figure 17. Unexploded ordnance - 81 mm mortar.



Figure 18 Unexploded ordnance - 90 mm M353 target practice round.



Figure 19. Unexploded 90 mm M353 projectile samples.



Figure 20. Unexploded 81 mm mortar samples.



Figure 21. Shrapnel samples from Limestone Hills.

The Montana Army National Guard has used the training area for live fire training since 1959. Types of ordnance found, or indicated by archival records to have been used at Limestone Hills include 76 and 90 mm TP-T (target practice with a tracer), AP/T (armor piercing tank), WP (white phosphorus), HE, 105 mm illumination, WP, HE, 4.2 inch illumination, HE, and 155 mm illumination, WP, and HE (Billings, 2004). The type of round from which the shrapnel samples originated cannot be identified.

8.1. Theoretical model

During the firing process, a given projectile does not reach a temperature above the Curie point of low carbon steel, 730° Centigrade (C) (Richards, 2004; Jubaraj Sahu, personal communication, May 11, 2006). However unexploded ordnance experiences a significant shock upon impact with the ground. This alters the magnetic properties of the ordnance, and may result in the magnetic domains becoming randomly aligned which would erase the original remanent magnetization (Billings 2004). Shrapnel is typically a rough, randomly shaped piece of steel created upon the impact and explosion of a projectile.

Remanent magnetization is the magnetization left in a sample after the external magnetic field is removed (Merrill et al., 1996). Viscous decay of remanence is the decrease of remanent magnetization with time in an external magnetic field, even if that field is constant. When an external field is applied

to and then removed from a sample, statistical thermal vibrations (Olhoeft 1972) within the domain structure cause metastable magnetic domains to experience an increase in activation energy. The domains which were previously held in place by energy barriers are now thermally activated over these barriers to reach a lower energy level. The magnetic remanence decays in this manner until an equilibrium state is reached within the sample (Crew et al., 1996, Dunlop & Ozdemir 1997, Mayergoyz et al., 1999). Acquisition or decay of magnetic remanence happens gradually over a period of seconds to millions of years depending on both grain size and temperature.

There are several sets of equations governing the acquisition or decay of remanent magnetization (Kok & Tauxe 1996). The first is known as the Neel Model (Neel 1949) and applies to single domain, uniaxial particles (Weller & Moser 1999).

$$M(t) = M_o e^{-t/\tau}$$

A second theory known as the Richter Model (Dunlop 1973) states that Viscous Remanent Magnetization (VRM) is acquired according to:

$$M(t) = M_o e^{-t/\tau} + M_{eq} (1 - e^{-t/\tau}),$$

where t is the time, and τ is the relaxation time or decay constant. This model applies to single domain particles or walls in multi-domain particles. The decay constant varies depending on the type of grains in the sample. For single domain grains the relaxation time τ is:

$$\frac{1}{\tau} = \frac{1}{\tau_o} \exp\left(\frac{-\mu_o V M_s H_k}{2kT(1 - \text{abs}(H_o) / H_k)^2}\right),$$

where $\tau_o = 10^{-9}$, μ_o is the magnetic permeability, V is the grain volume, M_s is the magnetic saturation, H_k is the microcoercivity, k is the Boltzman constant, and T is temperature (Nagata 1961). For multi-domain grains the relaxation time is:

$$\frac{1}{\tau} = \frac{1}{\tau_o} \exp\left(\frac{-c\mu_o V_{bark} M_s H_c}{kT}\right),$$

where H_c is the coercive force, V_{bark} is the Barkhausen volume, and c relates the maximum slope of a barrier to its height (a number of order unity; Nagata 1961).

In samples composed of many grains such as soil or shrapnel, a third theory works well to define the magnetic viscosity. In such samples logarithmic growth with time of the magnetization scaled by the coefficient of viscosity is exhibited (Street & Wooley 1949, Worm et al., 1991, Street & Brown 1994, Crew et al., 1996, Goodman et al., 2000):

$$M(t) = M_o + S \ln(t),$$

where S is the coefficient of magnetic viscosity and t is the exposure time to a given external magnetic field and M_o is the initial magnetization. The logarithmic trend occurs due to an ensemble of different grains shapes, sizes, and composition. This leads to a distribution of energy barriers for magnetic relaxation to overcome and results in a logarithmic decay of the remanence. While this is the most common experimental model, it indicates that VRM goes to infinity, which is not possible.

The logarithmic model is generally only observed over a restricted time interval (Kok & Tauxe 1996). It works well for intermediate time, but does not work for all time, the relation breaks down for small times and large times (Wohlfarth 1984, Mayergoyz et al., 1999, Williams & Muxworthy 2006). Kok & Taux (1996) state that data sets exist confirming all theories over restricted time intervals.

Another theory for viscous decay is known as the modified Richter model (Olhoeft 1972).

$$M(t) = M_o + \frac{C}{t + t_o},$$

where M_o is the initial magnetization, C is a constant, and t_o is the initial time. The modified Richter decay model is closest to the decay observed during this study which follows the relation:

$$M(t) = M_o + \frac{C}{\left[1 + \left(t/t_o^\alpha\right)\right]^\beta},$$

where M_o is the initial magnetization value, C is a constant, and β and α are real numbers.

8.2. Measurement process

Two visits to the Institute for Rock Magnetism (IRM) at the University of Minnesota occurred from April 21st to April 24th of 2006 and from August 20th to August 25th of 2006 respectively. During the first visit, the magnetic remanence of the shrapnel samples was characterized using the Princeton Applied Research vibrating sample magnetometer (PAR VSM). The parameters measured or derived from measurements are shown for two samples in Table 6.

Table 6. Hysteresis parameters for steel shrapnel samples.

Hysteresis Parameter	Sample C3	Sample R2
Maximum Field (Tesla)	1	1
Saturation Magnetization (kA/m)	154.8	246.0
Remanent Magnetization (kA/m)	4.47	18.2
Coercivity (kA/m)	1.32	1.33

Shrapnel sample C3 was also characterized during the second visit using the Princeton Measurements Corporation Micro Mag Vibrating Sample Magnetometer. The first parameter measured was the viscous remanent magnetization. The field applied to the shrapnel samples was 50 milliTeslas (mT) = 39.8 kA/m, while 250 mT = 199 kA/m was also used for sample C3 during the second visit.

The measurement procedure for the PAR VSM was as follows

- 1) Switch on the computer, lock-in amplifier, vibration control, and teslameter.
- 2) Turn on the precision bipolar magnet control.
- 3) Identify the short axis of the steel sample. Because the strength of magnetic moment is highly dependent on shape, the samples should be inserted into the PAR VSM with the short axis parallel to the applied magnetic field. The steel shrapnel samples are extremely magnetic and this orientation reduces the chance that the VSM will become overloaded upon application of the magnetic field.

- 4) Measure the weight of the sample and input this information along with a short description into the IRM VSM data acquisition system.
- 5) Attach the sample to the sample rod assembly securely with non-magnetic masking tape. There should be absolutely no ability for the sample to move out-of-phase with the rod.
- 6) Attach the sample rod to the sample rod assembly and tape the connection with masking tape to prevent rotation of the sample during the measurement process.
- 7) Toggle vibration control to the on position and apply the magnetic field.
- 8) Null the field, then observe and record the decay of the mass normalized magnetic moment for the desired time period.

C3 is the smallest of the shrapnel samples, and except for one flattened corner, the most cube-like. The sample does have one shorter axis and this axis was oriented parallel to the applied magnetic field. A 50 mT (= 39.8 kA/m) field was applied to the sample and then nulled. The sensitivity for this set of measurements was set to 1V, as the output was only approximately 0.5 V. VRM information was recorded for sample C3 (Figure 22) for 10,000 seconds (2 hours and 46 minutes).

For approximately the first 24 seconds the magnetic viscosity combines with the equilibration of the VSM to cloud the signal, thus analysis begins for $t \geq 24$ seconds. A logarithmic model provides the best fit for this sample:

$$M(t) = 0.0704 - 0.0031 \ln(t).$$

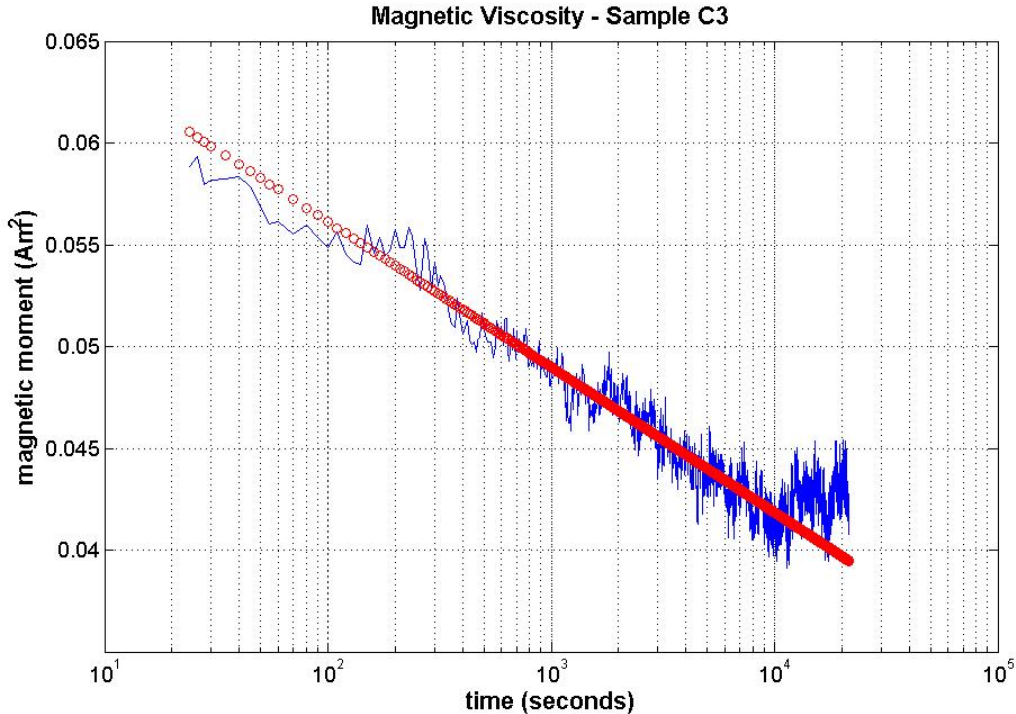


Figure 22. Magnetic viscosity measurements for shrapnel sample C3.

The projected decay for sample C3 was calculated for time periods extending out to 1000 years using a logarithmic model (Table 7).

Table 7. Projected decay times of magnetic remanence for shrapnel sample C3.

Sample C3			
Time Period	Time seconds	In Moment (Am²)	Percent Decay
12 hours	43200	0.037311853	47.00
1 day	86400	0.035163097	50.05
1 week	604800	0.029130775	58.62
1 year	31449600	0.01688192	76.02
10 years	314496000	0.009743906	86.16
100 years	3144960000	0.002605892	96.30
1000 years	31449600000	-0.004532122	106.44

In a period of 12 hours, this model predicts that the magnetic remanence will decay 47%, and in 100 years, 106% to a value with a negative dipole moment. This is obviously not a good model for viscous remanent decay at late times. In our second visit to the IRM (see later) we obtained better fits to the viscous decay curves using the Cole-Davidson model.

The hysteresis parameters for shrapnel sample C3 were successfully measured (Table 8). Using an applied field of 1T (=796kA/m) the sample reached magnetic saturation at 154.8 kA/m, the magnetic remanence value was 4.47 kA/m and the coercivity was 1.18 kA/m (Figure 23).

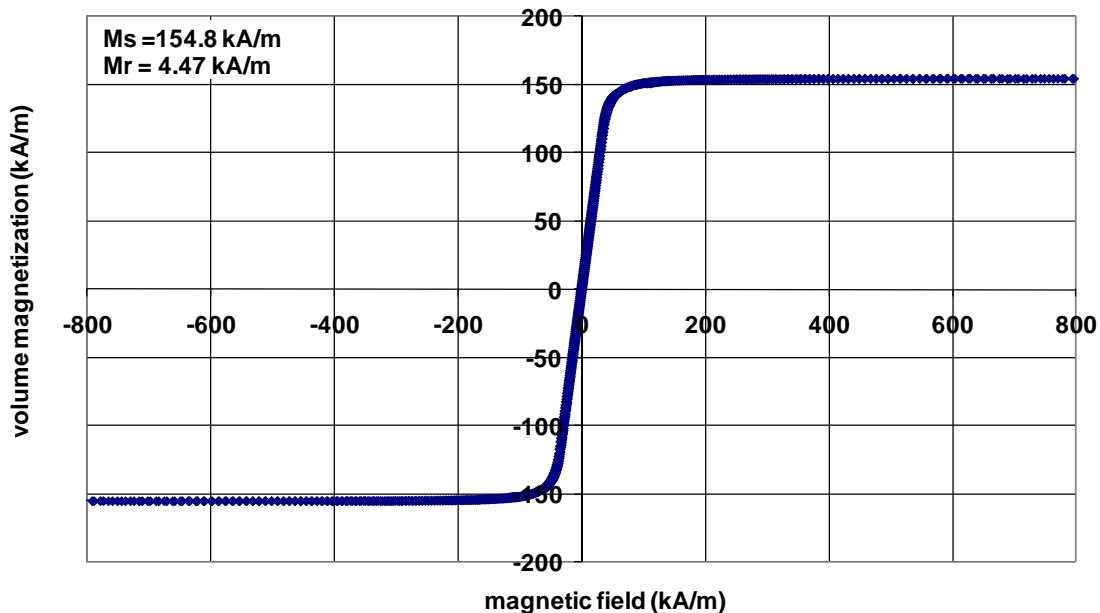


Figure 23. Hysteresis loop of shrapnel sample C3.

A second shrapnel sample to be measured was Random 2 or R2. This sample is totally random in shape. The sample does have one shorter axis and this axis was oriented parallel to the applied magnetic field. A 50mT (=39.8kA/m) field, again not quite a saturation field, was applied to the sample and then nulled. The lock-in amplifier did not overload upon application of the field. Data were recorded for sample R2 (Figure 24) for 10,000 seconds (2 hours and 46 minutes). For approximately 24 seconds the magnetic viscosity is clouded by the equilibration of the VSM, thus

analysis begins after this time period. The logarithmic model once again provided the best fit for the samples:

$$M(t) = 0.5838 - 0.0011 \ln(t).$$

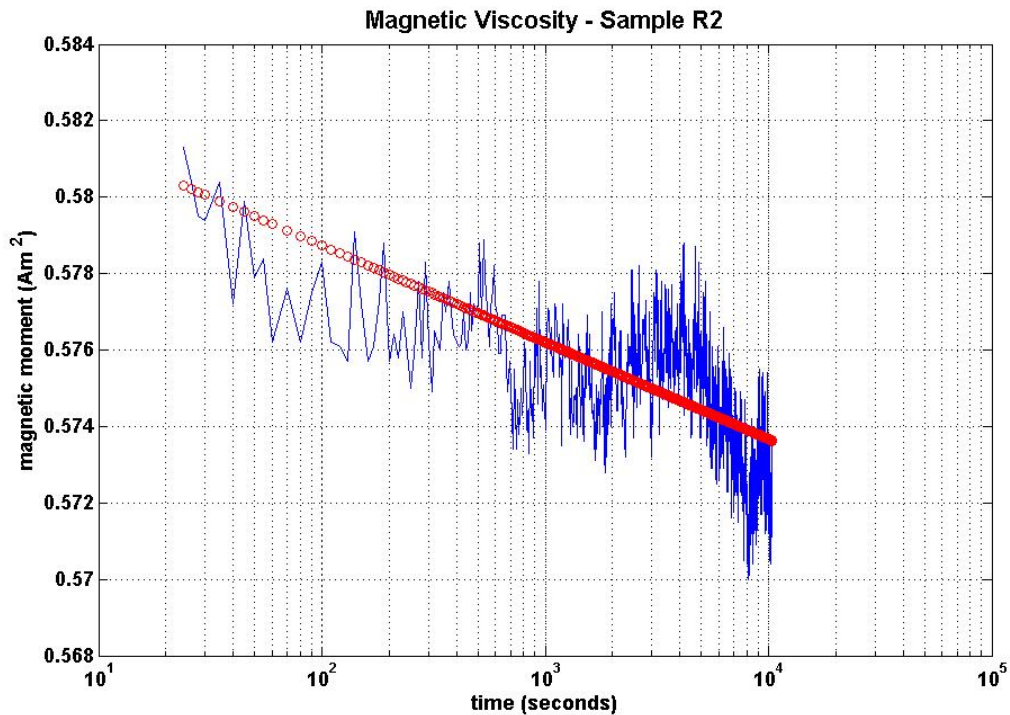


Figure 24. Viscous remanent decay for shrapnel sample R2.

The projected decay for sample R2 was calculated for time periods extending out to 1000 years using the logarithmic model (Table 7).

Table 8. Projected decay times of magnetic remanence for shrapnel sample R2.

Sample R2			
Time Period	In seconds	Moment (Am ²)	Percent Decay
12 hours	43200	0.5721	2.01
1 day	86400	0.5713	2.14
1 week	604800	0.5692	2.51
1 year	31449600	0.5648	3.26
10 years	314496000	0.5623	3.67
100 years	3144960000	0.5597	4.12
1000 years	31449600000	0.5572	4.55

In a period of 12 hours, this model predicts that the magnetic remanence will decay just 2%, and in 100 years, approximately 5%. Of all the shrapnel samples, the logarithmic model fits sample R2 the best.

The hysteresis loop for shrapnel sample R2 was successfully measured (Table 9). With an applied magnetic field of 1T (=796 kA/m) the sample reached magnetic saturation at 246 kA/m, magnetic remanence was 18.2 kA/m, and the coercivity measured 1.18 kA/m.

The published value of saturation magnetization for low carbon steel is 1,200 kA/m. At best, the measurements from IRM were about 20% of the published value. This difference is attributed primarily to corrosion of the shrapnel sample. In addition, it is unknown at what applied field the published value was obtained, and the method through which it was obtained. The published value of magnetic remanence for low carbon steel is 400 kA/m to 875 kA/m. At best the measured value of remanence was only about 5% of the published one. The difference is attributed again to the maximum applied field, and corrosion in the samples. The published values for coercivity range from 0.040 to 0.120 kA/m. The measured values were 5.25 kA/m, which is two orders of magnitude larger.

To ensure that the calculated decay trends were not just the product of the VSM itself, the viscous remanent magnetization of a paramagnetic sample was measured for approximately 1000 seconds (Figure 25). The sample consisted of 4659.3 mg of $MnCO_3$. The best fit line for this measurement:

$$M(t) = 2.2 \times 10^{-4}$$

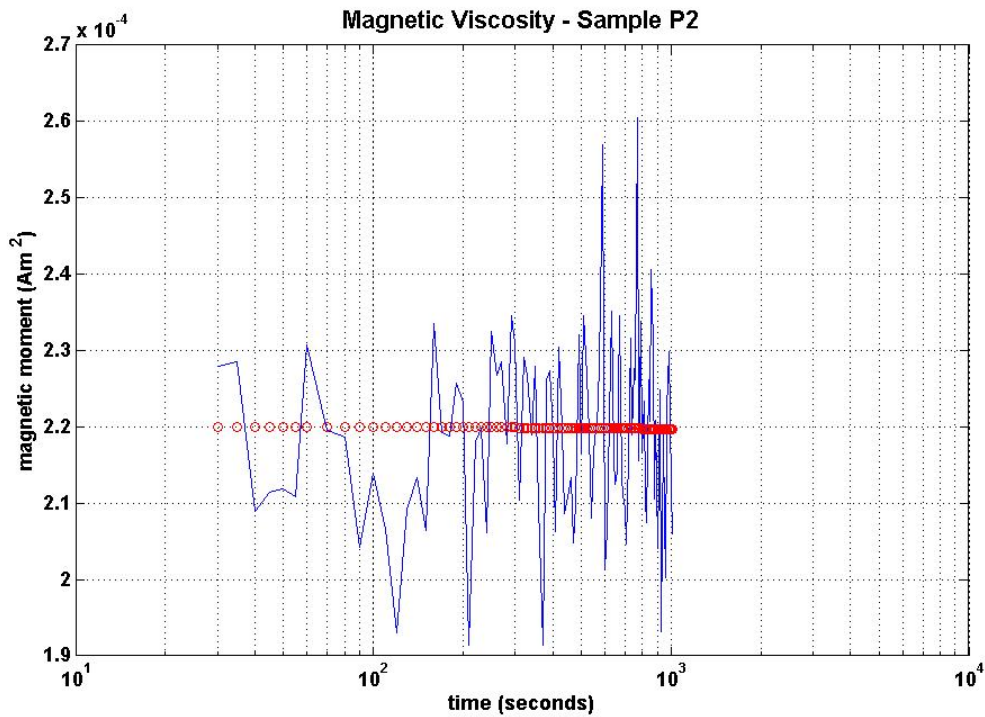


Figure 25. Viscous remanent magnetization for paramagnetic sample P2.

The readings for the paramagnetic sample simply oscillated about the magnetic moment of 2.2×10^{-4} Am² as expected, thus confirming that the measured decay of remanence was in fact a mechanism of the sample, and not an artifact from the vibrating sample magnetometer.

During the second visit to the Institute for Rock Magnetism, the magnetic remanence of fresh steel, unfired projectiles, and unexploded ordnance samples were characterized using the Princeton Measurements Corporation Micro Mag Vibrating Sample Magnetometer (PMC MM). The parameters measured or derived from measurements include viscous remanent magnetization of eleven samples, and the hysteresis loops including initial susceptibility, saturation magnetization, remanent magnetization, and coercivity of three samples (Table 9). In addition shrapnel sample C3 was characterized a second time. All samples were approximately cubic in order to account for the shape dependence of the measured values.

Table 9. Hysteresis parameters for fresh steel, unfired projectile, and unexploded ordnance samples.

Hysteresis Parameter	Fresh Steel Bar	81 mm Unfired	90 mm UXO
Maximum Field (kA/m)	198.9	795.8	198.9
Saturation Magnetization (kA/m)	76.82	123.7	121.7
Remanent Magnetization (kA/m)	1.73	6.40	3.11
Coercivity (kA/m)	4.52	14.09	0.844

Measurements began with two samples of fresh low carbon steel. As is the convention for this study, the short axis of each sample was aligned parallel to the applied magnetic field (198.9 kA/m). After removing the effect of VSM equilibration, the best model sample Bar 3 (Figure 26) proved to be Cole-Davidson in nature with the exception of the β -value which is greater than the defined range ($0 \leq \beta \leq 1$):

$$M(t) = 0.0616 + \frac{0.0015}{\left[1 + \left(t/t_o^{2.3}\right)\right]^{1.4}}$$

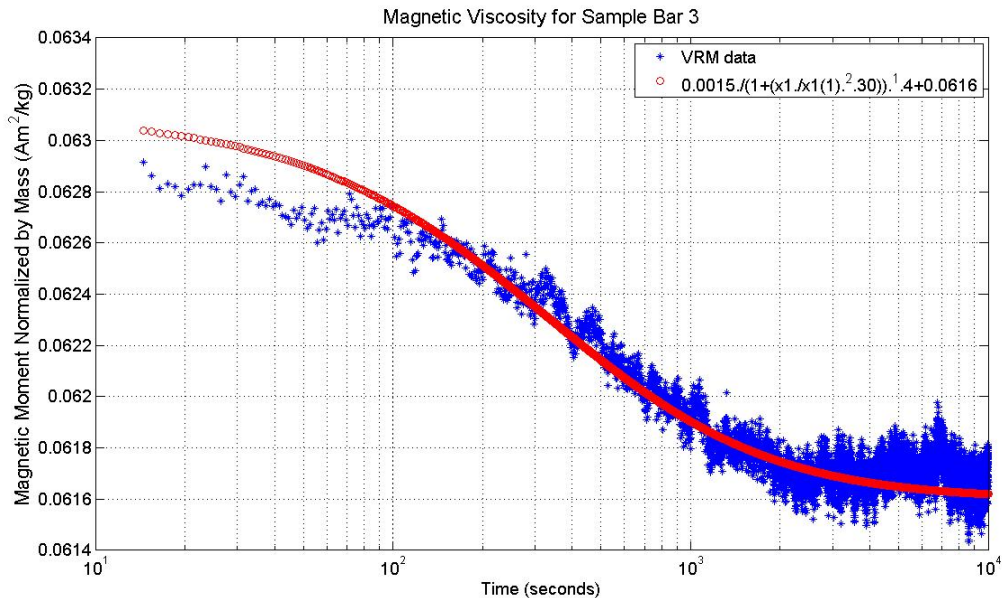


Figure 26. Cole-Davidson fit to magnetic viscosity measurements for sample Bar 3.

The two time ranges of interest for these measurements include 0 to 100 seconds (the measurement time for the MRIP), and “long times,” or the length of time between the emplacement of a piece of

unexploded ordnance, and the remediation time. The projected decay times for sample Bar 3 are presented in Table 10.

Table 10. Projected decay times for fresh steel sample Bar 3 using the Cole-Davidson model.

Sample Bar 3			
Time Period	In seconds	Moment (Am ²)	Percent Decay
100 seconds	100	0.062945388	0.24
12 hours	43200	0.061602662	2.37
1 day	86400	0.061601010	2.38
1 week	604800	0.061600066	2.38
1 year	31449600	0.061600000	2.38
10 years	314496000	0.061600000	2.38
100 years	3144960000	0.061600000	2.38
1000 years	31449600000	0.061600000	2.38

In the first range of interest, the decay is a mere 0.25%. This is good news as it verifies the assumption of the MRIP that the magnetic remanence will not change enough during the measurement process to affect the remanence value calculated from these measurements. On the second time scale of interest, the projected change in remanence for a period of 1000 years is only 2.38%. This, too, is encouraging as it verifies the assumption of the discrimination method of Billings (2004), magnetic viscosity will not cause a significant change in the magnetic remanence discrimination metric.

The hysteresis loop for the fresh steel was that of sample Bar 3 (Figure 27). The magnetic saturation measured 76.8 kA/m, the magnetic remanence 1.73 kA/m, and the coercivity 0.450 kA/m. The maximum applied field for the hysteresis measurements was 250 mT (=199kA/m).

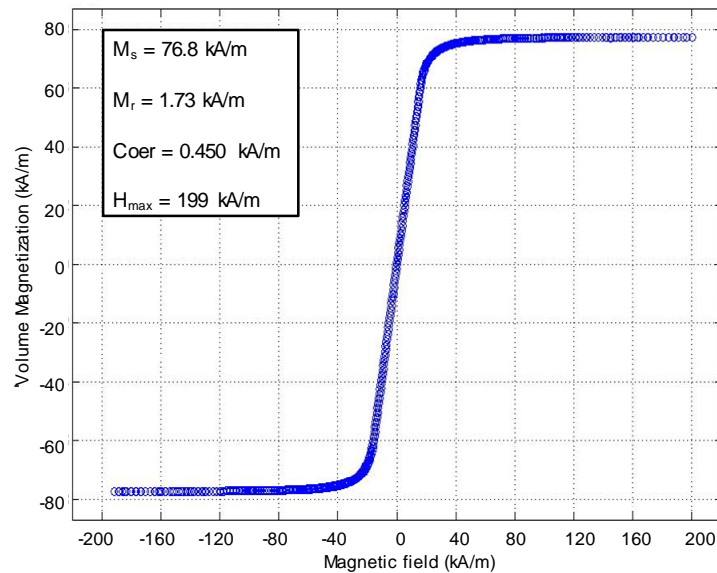


Figure 27. Hysteresis loop for fresh steel sample Bar 3 with a maximum applied field of 250 mT (199 kA/m).

The viscous remanent magnetization of two types of unfired projectile were measured, the first being an M821/M889 81 mm Mortar HE. This type of round is constructed from a steel alloy (HF-1). The sample was aligned parallel to the short axis, and a 250 mT (=199kA/m) field applied then nulled. The relaxation of the magnetic remanence again followed the Cole-Davidson trend. For sample 81-UN-2 (Figure 28) the best fit model was:

$$M(t) = 0.522 + \frac{0.021}{\left[1 + \left(t/t_o\right)^{2.305}\right]^{1.4}}$$

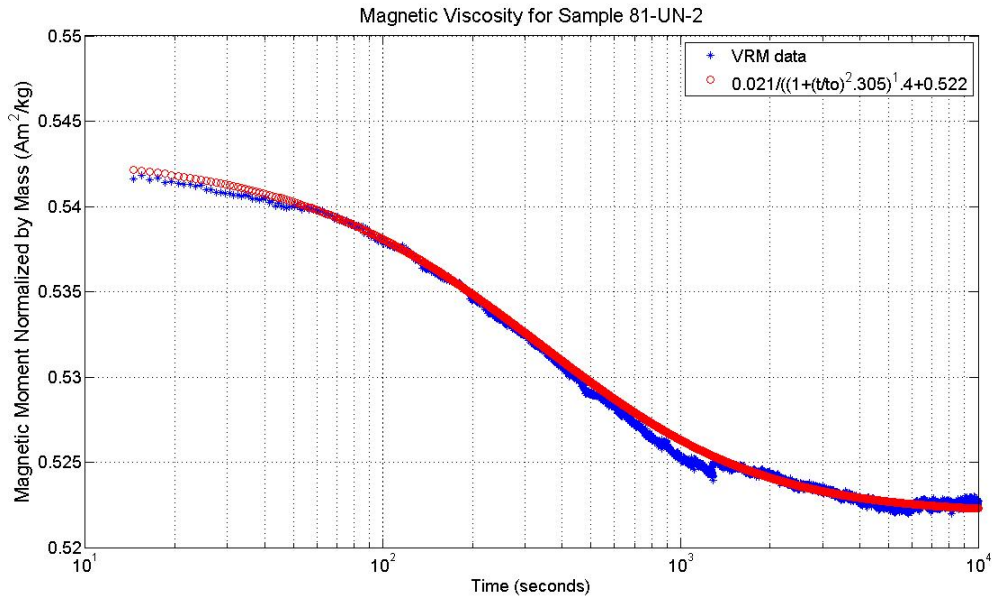


Figure 28. Magnetic viscosity measurements for sample 81-UN-2.

The projected decay of sample 81-UN-2 may be found in Table 11.

Table 11. Projected decay times of magnetic remanence for unfired projectile sample 81-UN-2 using the Cole-Davidson model.

Sample 81-UN-2			
Time Period	In seconds	Moment (Am ²)	Percent Decay
100			
seconds	100	0.540871508	0.39
12 hours	43200	0.522037974	3.86
1 day	86400	0.522014406	3.86
1 week	604800	0.522000946	3.87
1 year	31449600	0.522000004	3.87
10 years	314496000	0.522000000	3.87
100 years	3144960000	0.522000000	3.87
1000 years	31449600000	0.522000000	3.87

The decay in the first time range of interest is 0.39%, in the second time range it is 3.87 %. Again our two assumptions of interest are verified.

The hysteresis loop for the unfired projectile was that of 81-UN-2 (Figure 29).

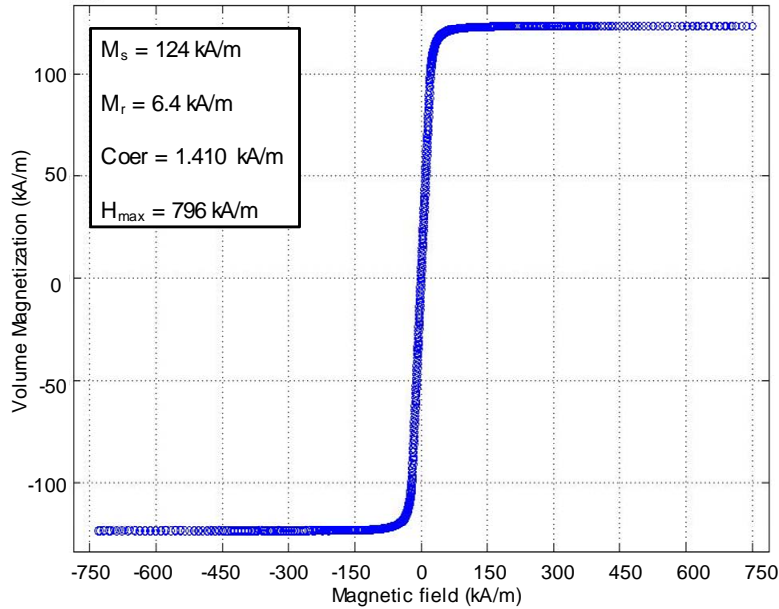


Figure 29. Hysteresis loop for unfired projectile sample 81-UN-2 with a maximum applied field of 1 T (796 kA/m).

The magnetic saturation measured 124 kA/m, the magnetic remanence 6.40 kA/m, and the coercivity 1.410 kA/m. The maximum applied field was 1 T (796 kA/m).

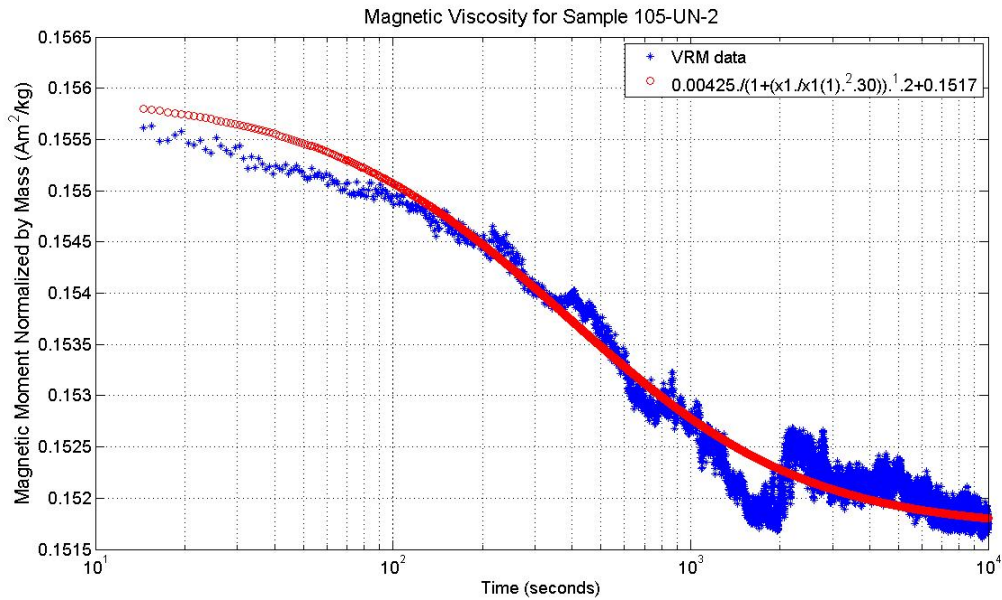


Figure 30. Magnetic viscosity measurements for unfired projectile sample 105-UN-2.

The second type of unfired projectile was the M1 105 mm HE. The round is constructed of low carbon steel AISI grade 1008. The sample was aligned parallel to the short axis and a 250 mT field was applied and nulled. The best fit Cole-Davidson model for sample 105-UN-2 (Figure 30):

$$M(t) = 0.1517 + \frac{0.00425}{\left[1 + \left(t/t_o^{2.3}\right)\right]^{1.2}}$$

It was not possible to measure the hysteresis loop for this sample as the mass was too large along with the dimensions of the sample.

In addition to the unfired projectiles, two types of unexploded ordnance were characterized with the Micro Mag. The first was a M353 90 mm TP-T constructed of low carbon steel ASTM A576. The sample was aligned parallel to the short axis and the 250 mT field applied then nulled.

The best fit Cole-Davidson model for sample 90-UXO-3 (Figure 31):

$$M(t) = 0.3005 + \frac{0.009}{\left[1 + \left(t/t_o^{2.3}\right)\right]^{1.5}}$$

The projected decay of sample 90-UXO-3 may be found in Table 12. The decay in the first time range of interest is 0.25%, in the second time range it is 3.22%. Our two assumptions of interest are verified. The hysteresis loop for the unexploded ordnance was that of 90-UXO-3 (Figure 31).

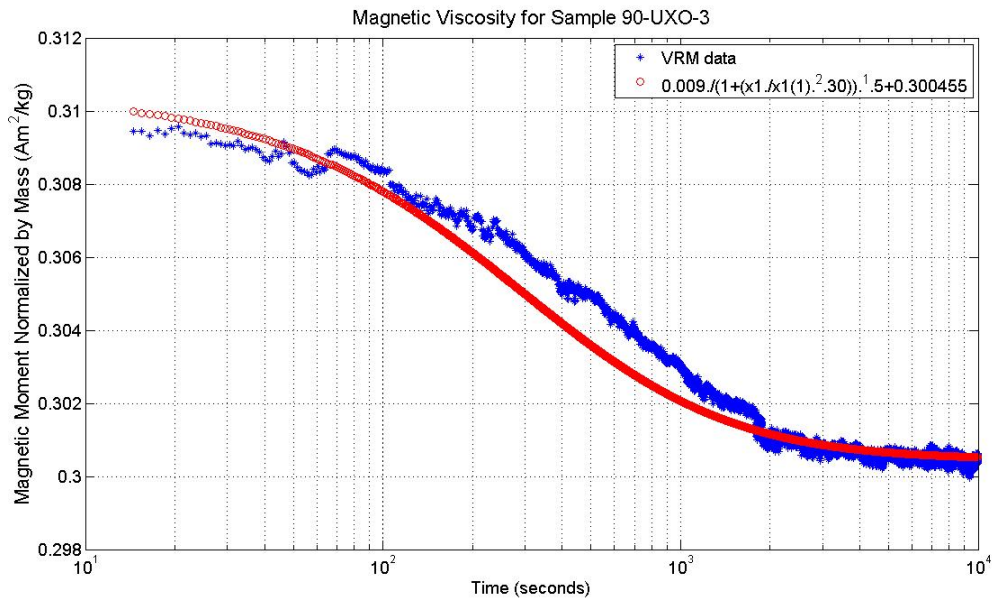


Figure 31. Magnetic viscosity measurements of unexploded ordnance sample 90-UXO-3.

Table 12. Projected decay times of magnetic remanence for unexploded ordnance sample 90-UXO-3 using the Cole-Davidson model.

Sample 90-UXO-3			
Time Period	In seconds	Moment (Am ²)	Percent Decay
100 seconds	100	0.309676981	0.25
12 hours	43200	0.300462190	3.22
1 day	86400	0.300457373	3.22
1 week	604800	0.300455105	3.22
1 year	31449600	0.300455000	3.22
10 years	314496000	0.300455000	3.22
100 years	3144960000	0.300455000	3.22
1000 years	31449600000	0.300455000	3.22

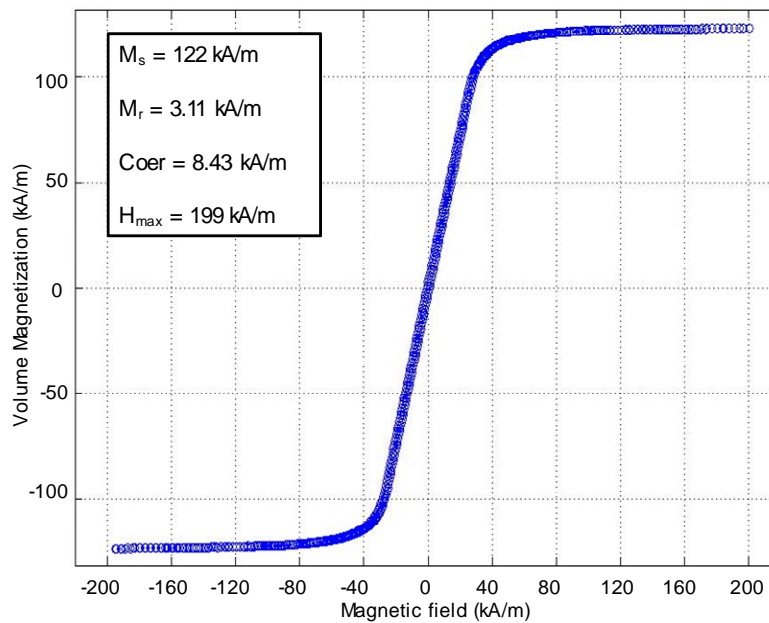


Figure 32. Hysteresis loop for unexploded ordnance sample 90-UXO-2 with a maximum applied field of 250 mT (=199kA/m).

The magnetic saturation measured 122 kA/m, the magnetic remanence 3.11 kA/m, and the coercivity 8.43 kA/m. The maximum applied field for the hysteresis measurements was 250 mT (=199 kA/m).

Finally the remanence of shrapnel sample C3 was re-characterized using the PMC MM. With the same orientation with respect to the magnetic field as was employed for the measurements with the PAR VSM, the magnetic viscosity was monitored for a period of 8,000 seconds. The best fit Cole-Davidson model for sample C3 (Figure 33):

$$M(t) = 0.4498 + \frac{0.015}{\left[1 + \left(t/t_o^{2.305}\right)\right]^{1.4}}$$

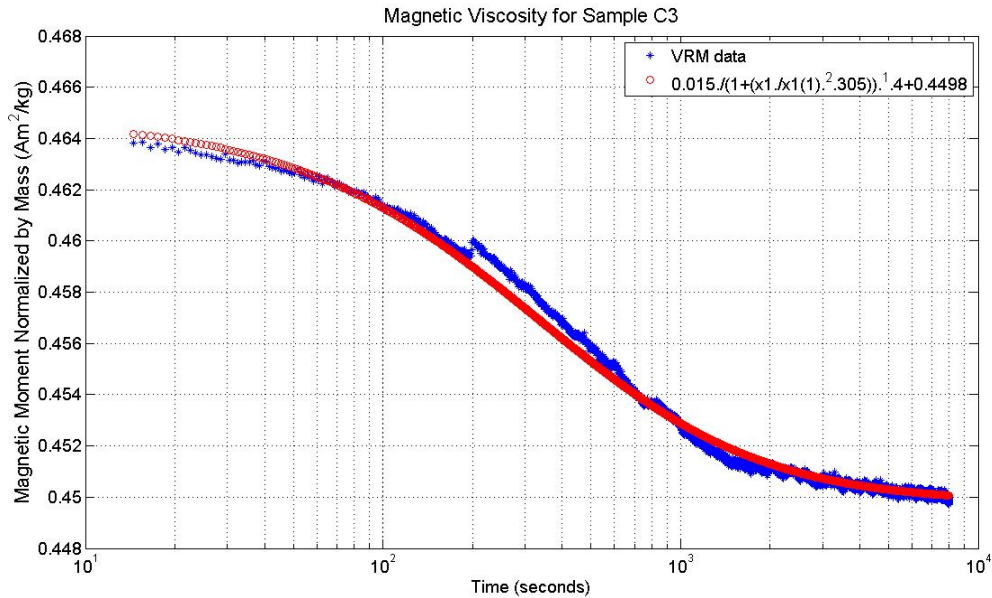


Figure 33. Magnetic viscosity measurements of unexploded ordnance sample C3.

The projected decay of sample C3 using the Cole-Davidson model may be found in Table 13.

Table 13. Projected decay times of magnetic remanence for shrapnel sample C3 using the Cole-Davidson model.

Sample C3 - 2			
Time Period	In seconds	Moment (Am²)	Percent Decay
100 seconds	100	0.463279648	0.33
12 hours	43200	0.449827125	3.22
1 day	86400	0.449810290	3.22
1 week	604800	0.449800675	3.23
1 year	31449600	0.449800003	3.23
10 years	314496000	0.449800000	3.23
100 years	3144960000	0.449800000	3.23
1000 years	31449600000	0.449800000	3.23

The decay in the first time range of interest is 0.33%, in the second time range it is 3.23%. Our two assumptions of interest are again verified.

The differences between the measurements of shrapnel sample C3 which occurred in April 2006, and those which occurred in August 2006 are these. The April measurements were made on the PAR VSM with an applied field of 50 mT (=39.8 kA/m). This field is not quite a saturation field. The best fit to the decay of remanence was the logarithmic model, however it broke down for late times. In contrast the August measurements of sample C3 were made with the PMC MM with an applied field of 250 mT (=199 kA/m). This field is a saturation field (or very close). For this dataset the best fit model is Cole-Davidson in nature. It fits the data well at all times, specifically providing a very good fit at long times.

The Cole-Davidson model of viscous remanent magnetization is better than the logarithmic model for the fresh steel, unfired projectile, unexploded ordnance, and shrapnel samples. In agreement with the Cole-Davidson, each sample exhibits a slow initial decay, followed by a fast intermediate decay which then stabilizes at later time. The model fits for all times, not just intermediate times as in the case of the logarithmic model.

The fact that the Cole-Davidson model is the best fit indicates that the samples have a distribution of relaxation times. Magnetic domains align when a magnetic field is applied. When the field is removed, some domains move more quickly back towards their equilibrium state than others. This is due to the fact that steel is comprised of several elements, all with different relaxation times. There are many different sizes of magnetic domains within steel, again, all with different relaxation times. Grains within a given sample may be single or multi-domain. All the domains within a multi-domain grain may not relax at the same rate, thus broadening even further the distribution of relaxation times.

See the next section for the final conclusions regarding magnetic viscosity.

9. Summary and Conclusions

9.1. Summary

The promising discrimination results achieved in the Montana case-studies described in Billings (2004) provided the impetus for this current study. At the Montana sites a prioritization of the digging order using apparent remanence would have resulted in the recovery of all UXO with 70% of non-hazardous items (shrapnel, cultural debris etc) left in the ground. There were differences in the apparent remanent magnetization of seeded and live-site UXO indicating that our conceptual understanding of remanence in UXO was incomplete. As the discrimination technology would result in certain detected items being left in the ground, a comprehensive understanding of the physical phenomena was deemed necessary.

As part of this project we developed a mobile device, the Magnetic Remanence Interrogation Platform, or MRIP, for measuring the induced and remanent moments of steel samples. The MRIP comprises six three-component fluxgate magnetometers symmetrically distributed around a rotating sample holder. Samples are placed on the holder and are slowly spun through two complete rotations. The measurement is repeated after the sample is physically rotated by 90° so that the previous up direction points east. The MRIP platform was deployed to two field sites (Limestone Hills and Camp Sibert), as well as to the Aberdeen Test Center where measurements were made on 81 mm mortars before and after firing. At Limestone Hills the one-hundred and forty-nine 76- and 90-mm projectiles were measured. Most had relatively low remanent magnetization relative to the induced, suggesting that shock demagnetization occurs. Variations in the remanent moments of different specimens of 90-mm projectiles were attributed to variations in the type of steel used. There was a strong correlation of the direction of remanent and inducing field during burial, indicating evidence of shock magnetization and/or magnetic viscosity. At the second site, intact and partial 4.2-in mortars as well as shrapnel, base plates, and cultural debris were measured. Most of the base plates and intact mortars had low remanent magnetization, whereas the shrapnel and partial mortars tended to have higher remanent magnetization.

At ATC the MRIP device was used to make measurements of the magnetic remanence of sixty-five 81 mm mortars before firing and after impact. As delivered, 64 of the 65 rounds had very low remanent magnetization and a magnetizer had to be used to impose various amounts of remanence on the mortars. Three different categories of initial remanent magnetization were created (low, medium and high remanence) and these were fired at three different charge increments (0, 1 and 2 charge increments). The mortars that initially had low remanent magnetization acquired a magnetization in the direction of the inducing field, with the amount of shock magnetization decreasing with increasing impact velocity. The mortars with medium and high initial magnetization all lost some of their magnetic remanence with the amount increasing with increasing impact velocity (from ~50% at 0 charge increment to ~70% at two charge increments). Even at the highest impact velocity, shock demagnetization of initially highly magnetized mortars was insufficient to guarantee effective discrimination using apparent remanence.

During the project, two visits were made to the Institute for Rock Magnetism for the purpose of measuring the magnetic properties (in particular the magnetic viscosity) of a number of steel samples.

The magnitude of magnetic viscosity for fresh steel, unfired projectiles, unexploded ordnance, and shrapnel was quite similar at less than 1.5% decay for the time scale of interest for the MRIP, and less than 6% decay for all time brackets up to 1000 years with an average of 3.38% decay. The viscous decay of the unfired projectiles was slightly higher than that of the UXO, shrapnel, and fresh steel, but only by about 2%. In short, magnetic remanence persists longer than the time scales of interest. It is stable for time scales of up to one thousand years, quite likely even longer. For this study the magnetic viscosity will not hinder the ability of the MRIP to resolve the magnetic remanence of a given UXO. In addition, the results of this experiment have an important implication; magnetic viscosity is not relevant to the magnetic discrimination process.

9.2. Conclusions

The main conclusion of this project is that **discrimination using apparent remanence is not reliable enough to guarantee the excavation of all detected UXO**. In the live-site measurements at Camp Sibert and the controlled firing tests at ATC (this report) several ordnance items possessed sufficient magnetic remanence to confound the apparent remanence metric ranking scheme. The measurements made at Limestone Hills suggest that apparent remanence might be more reliable for direct fired artillery projectiles that presumably suffer a larger shock on impact. However, even at Limestone Hills, there was a least one outlier with relatively high magnetic remanence. Therefore, we can never guarantee that sufficient demagnetization occurs so that apparent remanence discrimination will be reliable. There is simply too much potential variability in both the initial magnetic remanence and shock regime experienced by a projectile. For example, consider the case where a direct fired round skips and tumbles several times before coming to rest and never suffers a large shock. Or where an indirect fired round impacts an easily penetrated soil (such as the silty-loam soils encountered at ATC) instead of a nearby rock outcrop.

The Limestone Hills and Camp Sibert field measurements, along with the earlier Montana case-studies, demonstrate that apparent remanence is an effective method to recover 95% or more of the unexploded projectiles without the need to excavate all the detected shrapnel, range debris and cultural junk. Thus apparent remanence could provide an effective ranking strategy in applications where not all detected anomalies can be excavated. This includes marine applications where the expense of excavating a single anomaly typically prevents all detected anomalies from being investigated. Another application is in the interpretation of HeliMAG data collected for wide-area-assessment. Billings & Wright (2009) interpreted HeliMAG data collected at the Yekau Lake site near Edmonton, Alberta, and found that target density estimates generated by considering all detected anomalies provided some evidence of bombing activity, but were inconclusive as to the specific location of the suspected 11.5 pound bomb target. They calculated the apparent remanence metric for each detected anomaly and discarded detections where the apparent remanence was greater than 75%. The revised target density estimates clearly delineated the presence and spatial extent of the bombing target, and several intact 11.5 pound bombs have been found in that area.

For those applications where 100% recovery of detected UXO is required an alternative ranking scheme based on the size of the magnetic moment is preferred. As shown in the Camp Sibert discrimination study (Billings et al. 2008) ranking by moment provided a reliable method for discrimination of intact 4.2" mortars from non-hazardous items. The method was reliable but not

particularly effective, because many favorably oriented small targets had to be excavated to ensure recovery of unfavorably oriented 4.2” mortars (those oriented perpendicular to the Earth’s field). Additionally, many scrap items with large remanent magnetization had to be excavated as suspected UXO, because no information on the orientation of the magnetization is used when ranking by dipole moment alone.

Summarizing other relevant results from this study:

- 1) **Shock demagnetization:** The controlled firing tests at ATC demonstrate that Altshuler’s (1996) hypothesis that shock demagnetization occurs in ordnance was correct. As intuitively expected the amount of demagnetization increases with increasing impact shock. However, the maximum impact velocity achieved at ATC (210 m/s) was insufficient to completely erase the preexisting remanence of the 81 mm mortars that had a high initial magnetic remanence. The field measurements at Limestone Hills are suggestive of almost total shock demagnetization of indirect fired projectiles that impact at high velocities. However, the initial remanence of these projectiles is unknown and a plausible alternative explanation is that the rounds never possessed remanence in the first place.
- 2) **Shock magnetization:** The live-site measurements at Limestone Hills provided indications (but not compelling evidence) that rounds acquire remanence in the direction of the inducing field at the time of impact (shock magnetization). The controlled tests at ATC conclusively demonstrated that shock magnetization of rounds occurs. Rounds that initially started with a very small remanence acquired a magnetic remanence in the direction of the inducing field at the time of impact. In addition, rounds with high initial remanence lost some of that remanence and appeared to be progressing towards a similar final state of remanence as the rounds with low initial remanence.
- 3) **Magnetic viscosity:** The magnitude of magnetic viscosity for fresh steel, unfired projectiles, unexploded ordnance, and shrapnel was quite similar at less than 6% decay for all time brackets up to 1000 years with an average of 3.38% decay. Magnetic remanence persists longer than the time scales of interest. It is stable for time scales of up to one thousand years, quite likely even longer, indicating that magnetic viscosity is not relevant to the magnetic discrimination process.

10. References

- Altshuler, T. W., 1996, Shape and Orientation Effects on Magnetic Signature Prediction for Unexploded Ordnance: in *Proceedings, 1996 UXO Forum*, Williamsburg, VA.
- Billings, S. D., 2004, Discrimination and Classification of Buried Unexploded Ordnance Using Magnetometry: *IEEE Transactions on Geoscience and Remote Sensing* **42**, 1241 – 1251.
- Billings, S. D., 2009, Field measurements of induced and remanent moments of unexploded ordnance and shrapnel: *IEEE Transactions of Geoscience and Remote Sensing*, **47**, 815-827.
- Billings, S. D., Pasion, L. R. and Oldenburg, D.W., 2002, Inversion of Magnetics for UXO Discrimination and Identification: in *Proceedings, 2002 UXO Forum*, Orlando.
- Billings, S.D., Pasion, L. R., Berans, L., Oldenburg, D. W., Lhomme, N., Song, L. P., Sinex, D., Kingdon, K. and Jacobson, J., 2008, Data Modeling, Feature Extraction, and Classification of Magnetic and EMI Data, ESTCP Discrimination Study, Camp Sibert, AL, Project 200504: Practical Discrimination Strategies for Application to Live Sites, Demonstration Report. ESTCP Program Office.
- Billings, S. D., Pasion, C, Walker, S. and Beran, L., 2006, Magnetic models of unexploded ordnance: *IEEE Transactions of Geoscience and Remote Sensing*, **44**, 2115- 2124.
- Billings, S. D. and Youmans, C., 2007, Experiences with unexploded ordnance discrimination using magnetometry at a live-site in Montana: *Journal of Applied Geophysics*, **61**, 195-205.
- Billings, S. D. and Wright, D. W., 2009, Interpretation of high-resolution low altitude helicopter magnetometer surveys over sites contaminated with unexploded ordnance: *Journal of Applied Geophysics*, (submitted).
- Blakely, R. J., 1996, Potential Theory in Gravity and Magnetic Applications: Cambridge University Press.
- Calderwood, J.,H., 2003, A physical hypothesis for Cole-Davidson Behavior: *IEEE Transactions on Dielectrics and Electrical Insulation*, **10**, (6), 1006-1011.
- Crew, DC, McCormick, PG, and R Street, 1996, The interpretation of magnetic viscosity: *Journal of Physics D: Applied Physics*, **29**, 2313-2319.
- Davidson, D., W., and R. H. Cole, 1951, Dielectric Relaxation in Glycerol, Propylene Glycol, and n-Propanol: *The Journal of Chemical Physics*, **19**, (12), 1484-1490.
- Defense Ammunition Center (DAC), 2006, MPTS PROJ 90MM TP-T M353 - DAC – MIDAS detailed structure for an item: Munition Items Disposition Action System (MIDAS), Defense Ammunition Center.
- Dunlop, David J., 1973, Theory of the magnetic viscosity of lunar and terrestrial rocks: *Reviews of Geophysics and Space Physics*, **11**, (4), 855-901.
- Dunlop, David J., and Ozden Ozdemir, 1997, *Rock Magnetism – Fundamentals and Frontiers*: Cambridge University Press, 571p.
- Goodman, AM, Laidler, H, O’Grady, K, Owen, NW, and AK Petford-Long, 2000, Magnetic viscosity effects on the pinned layer loop of spin-valve materials: *Journal of Applied Physics*, **87**, (9), 6409-6411.

- Kok, Y. S., and L. Tauxe. 1996. "Saw-toothed Pattern of Relative Paleointensity Records and Cumulative Viscous Remanence," pp. 95-99 in *Earth and Planetary Science Letters*, Vol. 137.
- Mayergoyz, ID, Adly, A, Korman, C, Huang, Mingwei, and C. Krafft, 1999, Scaling and data collapse in magnetic viscosity: *Journal of Applied Physics*, **85**, (8), 4358-4360.
- Merrill, Ronald T., McElhinny, Michael W., and Phillip L. McFadden, 1996, *The Magnetic Field of the Earth - Paleomagnetism, the Core, and the Deep Mantle*: Academic Press, Inc., 531p
- Nagata, T. 1961. *Rock Magnetism*. Tokyo: Maruzen.
- Nagata, T. and B. J. Carleton. 1969. "Notes on Piezo-remanent Magnetization of Igneous Rocks II," *J. Geomag. Geoelectr.* **29**: 427-445.
- Néel, L., 1949, Théorie du traînage magnétique des ferromagnétiques en grains fins avec applications aux terres cuites: *Annales Géophysique*, **5**, 99-136.
- Nelson, H. H., Altshuler, T. W., Rosen, E. M., McDonald, J. R. Barrow, B. and Khadr, N., 1998, Magnetic Modeling of UXO and UXO-like Targets and Comparison with Signatures Measured by MTADS: in *Proceedings, 1998 UXO Forum*, Anaheim, CA.
- Olhoeft, Gary, 1972, Time dependent magnetization and magnetic loss tangents: Masters Thesis at the Massachusetts Institute of Technology, 94p.
- Richards, Austin, 2004, Applications for High-Speed Infrared Imaging: SPIE International Congress on High-speed and Photonics N°26, Alexandria VA , Proceedings, vol. 5580, pp. 137-145.
- Jubaraj Sahu, Army Research Laboratory, personal communication, May 11, 2006.
- Stratton, J. A., 1941, *Electromagnetic Theory*: McGraw Hill.
- Street, R, and SD Brown, Magnetic viscosity, fluctuation fields, and activation energies: *Journal of Applied Physics*, **76**, (10), 6386-6390.
- Street, R, and JC Woolley, 1949, A study of magnetic viscosity: *Proceedings of the Physical Society Section A*.
- Trinchenko, O., Billings, S. D. and Nigma, N, 2009, Modeling of shock induced changes to the magnetization of unexploded ordnance, Project MM-1380 Final Report supplement: SERDP Program Office.
- Weller, Dieter, and Andreas Moser, 1999, Thermal effect limits in ultrahigh-density magnetic recording: *IEEE Transactions on Magnetics*, **35**, (6), 4423-4439.
- Williams, Wyn, and Adrian R. Muxworthy, 2006, Understanding viscous magnetization of multidomain magnetite: *Journal of Geophysical Research*, **111**, B02102.1-B02102.13.
- Wohlfarth, EP, 1984, The coefficient of magnetic viscosity: *Journal of Physics F: Metal Physics*, **14**.
- Worm, HU, Jackson, M, Banerjee, SK, and CM Schlinger, 1991, Magnetic viscosity of single domain magnetite particles: *Journal of Applied Physics*, **70**, (10), 5533-5537.
- Young, C.W. 1997. *Penetration Equations*. Sandia Contractor Report SAND97-2426. Albuquerque, NM: Sandia National Laboratories.

Appendix A: Field diary for ATC firing tests

Sky Research personnel involved in the field test were Stephen Billings (PI) and Matt Ragusa, with Laurens Berans of UBC-GIF assisting. ATC personnel involved in the test included Larry Overbay (Point of Contact), Russell Yocum and Geoff Cunningham.

Tuesday May 27 2008

We arrive at ATC at 7AM, obtain badges and then go to the NDE laboratory at ATC and meet Russell Yocum who will help us magnetize the mortars and projectiles. Larry has to coordinate with Janet Simms and her ERDC crew so leaves another guy, Geoff, to help us out. It's a slow morning, so we went over to an equipment rental center and pick up a large 20 foot by 20 foot tent with aluminum poles for protecting the MRIP. Later in the day, we select a set-up location which is in a grassed area near the NDE laboratory. It takes a while to set-up as we are not allowed to put in stakes until Larry returns with a Schonstedt to sweeps the area. By the end of the day, we have the tent and table set-up but did not get a chance to collect any test-data.

Wednesday May 28 2008

This is a long and frustrating day. We finish setting up the MRIP and start measuring rounds, but notice some problems with the encoder. We also had the sensors a little too far from the table center. Matt had left the spare encoder back at the hotel so we had to drive back to pick it up. The new encoder doesn't appear to fix the problem, as the encoder keeps sticking and is not indexing properly. We spend a lot of time trying to resolve the problem and in the end take the DAS and encoder back to the hotel. Matt finds that the encoder works fine in his room.

Thursday May 29 2008

We discover that it's the encoder mount that is the problem and resolve the issue by attaching the shaft of a working encoder to the sample holder axis. It requires a fair amount of duct tape but appears to work quite well. We then get all the 81 mm mortars and start measuring them. For each round, we use a dremel tool and engrave a number (between 1 and 60), on the round, and also engrave a reference point near the tail of the round (where the aluminum tail mounts to the steel body). We do two rotations of each round with a static measurement every time we switch rounds. We manage to collect data over all 60 mortars and do the standard calibration coil measurements. We find that all the rounds, except 1 have very little remanent magnetization.

Friday May 30 2008

We spend the day magnetizing items in the NDE laboratory. We tried to get two categories of axial and two categories of transverse magnetization. We managed to impose a relatively large remanence in the axial direction, as well as a second smaller amount of remanence. For the transverse magnetization, we could only manage to get one category of modest remanent magnetization.

The procedure used was a little ad-hoc. Rounds were hand-held in the coil which was energized. For the axial magnetization we alternated directions so that we could have samples magnetized towards the nose of the mortar and others magnetized towards the tails. After magnetization, each round was measured with the MRIP. There were several rounds that weren't properly magnetized and these had to be returned to the NDE laboratory and the magnetization process repeated.

Three different pieces of equipment were used: one for the moderate transverse and strong axial magnetizations, another for the moderate axial magnetizations, with a third, larger and more powerful unit, used for the large transverse magnetization. This latter instrument, did not create a larger magnetization in the transverse direction that the first instrument. Ideally I would have liked to

have adjusted the magnetizations of several rounds, but it was a Friday and the NDE laboratory closed at 3 PM.

Monday June 2 2008 day 154

The 81 mm mortars were transported over to Edgewood on the weekend, so there is no chance we can adjust their magnetization. We pack up the tent and table and then head back to the hotel to wait for Larry to finish with the ERDC tests. This takes a while and it's close to 4PM before we meet and drive over to Edgewood to set-up the MRIP. We find a good spot right next to firing point 3. There are a couple of large sheets of metal nearby but we manage to find a quiet location in the middle of them. We set-up, then take some basic calibration measurements before heading back to the hotel.

Sensors 2 and 4 were mistakenly switched for this set-up.

Tuesday June 3 2008 day 155

Sensors 2 and 4 were mistakenly switched for this set-up.

Early start today with a 6AM meeting time at a spot close to the Edgewood security gate. We have to fill out some extensive paperwork to enter Edgewood, so that it's after 7AM before enter. We drive to the ammo dump and discuss logistics with the EOD techs, then drive to firing point 3 to get MRIP primed and ready. The EOD tech brings over half the rounds, which we measure (with one rotation). He then comes and picks those up (so he can take them back to the ammo-dump and attach the ignition cartridges), and drops off the other half. We managed to get all 65 rounds measured before it's time to fire the rounds (there were 5 extra rounds that we mark with the dremel tool and measure for the first time). For round 65, I struck it several times with a hammer while it was oriented with the Earth's magnetic field so that I could impose a magnetic remanence on it.

The gun-crew arrives around 10 AM and starts to set-up. We do charge #1 first, these were all fired in order and comprise numbers 43 to 63. It took a few spotting rounds before the mortars started to land in the right spot. Firing started at around 11:45 AM and was complete by 1:05PM. We then broke for lunch. After lunch, the gun-crew decided to move positions and do the 0 increment shots as they only had one spotter left. The new position was immediately adjacent to I-field. You could follow each round as it went up into the air, tipped over, then came back down again and landed. After a few minor adjustments after the first few rounds, the remaining mortars were shot very quickly. The last three were sent literally one after another and all were in the air at the same time (this was a bit of grand-standing by the gun-crew chief). These charge 0 rounds were fired in order and comprised rounds 1 to 21. Firing took place from about 2:05 PM to 2:20 PM.

Spotters in a tower near I-field monitored the impact positions of each mortar, and then marked each impact hole with a red-flag. They managed to locate all 42 rounds fired today.

Wednesday June 4 2008 day 156

Sensors 2 and 4 were mistakenly switched for this set-up.

Arrive at Edgewood about 9:15 AM, and then head out to firing point 3 where the gun-crew have set the mortar up ready to fire. It takes one spotter to bracket the impact area using 2 charge increments, so they immediately commence firing. This time, they make sure the notch is pointing up when they drop the round into the mortar tube. All 23 rounds (we had 2 spares) were fired and their entry points marked by spotters in the tower adjacent to I-field. Charge 2 rounds comprised numbers 22 to 42 and rounds 64 and 65 and all the entry points were found by the spotters.

It had rained heavily overnight and the tent had fallen down and broken the mount for sensor 5. Matt glues the base-plates back together so we can reattach sensor 5.

In the afternoon, we head over to I-field and start excavating the charge 0 rounds (most were sticking up out of the ground), while an excavator operator and EOD-tech start to dig up the charge 2 rounds. For all the charge 0 rounds I take various measurements including: orientation of round,

azimuth of notch, dip of round (from vertical), depth to the top of the tail fin (or height above ground).

The mortars have a fuze on them and not all the fuzes detonated on impact, which could create a safety hazard. We decide to move the MRIP over to I-field so that we won't have to transport the rounds before measurement. Laurens and Matt go get the MRIP and we set in up near the charge 0 rounds, hopefully far enough away from the excavator and any traffic on the I-field access track. We just finish setting up the table when we have to leave the site due to storm warnings. We secure a tarp over the table and as we start to drive away the heavens open and heavy rain commences.

Thursday June 5 2008 day 157

Sensors 2 and 4 were mistakenly switched for this set-up.

Arrive at Edgewood at around 8 AM. Some Army EOD guys looked at the fuzes on the rounds and decided that they could take them off safely and leave them in a pile for detonation next week. They first dealt with the charge 0 and 2 rounds that had been excavated the day before, and returned after lunch to neutralize the remaining charge 2 rounds as well as all the charge 1 rounds.

Larry, Geoff, Doug and two gunners continue excavating charge 1 rounds which Stephen measured. An EOD-tech worked with an excavator operator to extract the remaining charge 2 rounds. Some of these were found 6 feet beneath the ground. Some of the charge 1 rounds (43, 45, 46, 47, 48, 51, 54, 58, 59, 62) were extracted with the excavator. 64 of the 65 rounds were recovered: round 33 was the only one that couldn't be found.

While the excavating was occurring, Laurens and Matt started operating the MRIP. We ran the system without sensor 5 and just a small tarp over the table to protect the sensors from the sun. They ran all the charge 0 rounds and some of the charge 2 rounds (including some with fuzes that had sheared off) before lunch. After lunch, Stephen started to help as well and the remaining rounds were measured. The rounds measured during the first data collection event after lunch had to be measured again as data were not recorded for sensors 4 and 6.

I conducted a little experiment on mortars 7 and 15. Mortar 7 had a low magnetization, so I aligned it with Magnetic North and had it dipping at 65 degrees so it was parallel to the Earth's magnetic field, then I struck it with a hammer. Mortar 15 had high remanence, so I put it perpendicular to the Earth's field and also struck it with a hammer. The rounds were measured again afterwards.

We packed up all the equipment into two pickups and left the site at around 5:30PM.

Friday June 6 2008

Laurens and Matt meet up with Geoff at Aberdeen and pack all the equipment in a shipping crate ready for transport back to the Sky facility in Denver, CO.

Appendix B: Theory of shock induced changes to magnetization

1 Introduction

It has been known for a long time that hitting a nail in the presence of the Earth's magnetic field with a hammer without destroying the nail, causes the magnetization of this nail to be in the direction of the Earth's field. This is how compasses can be made. This relationship between mechanical stress and magnetization, also called magnetomechanical effect, has been documented in literature as seen in the review paper, [20].

As part of this project, we attempted to develop a semi-quantitative model that could be used to estimate the change in magnetization caused by a given applied stress. We were not successful in meeting this objective: our modeling attempts were insufficient to quantitatively explain the results of the measurements made in the field and controlled firing tests presented earlier in this document. Rather than describing the modeling efforts in detail, we will here concentrate on reviewing the basic principles behind the theory of shock induced changes to magnetization. This material will hopefully serve as a good starting point for future research into this area.

1.1 Conceptual Model

There are three predicted scenarios for changes in the remanent magnetization of UXOs between the time of firing and impact, or detonation. The three scenarios are illustrated in Figures 1 to 3. The three scenarios include:

1. As a result of the manufacturing process the casing of UXO are permanently magnetized and acquire thermoremanent magnetization. After firing, impact, and penetration without detonation, the ordnance can become demagnetized, or the remanent magnetization can be reduced. Over time, the UXO and shrapnel acquire a viscous remanent magnetization that is preferentially oriented in the same direction as the inducing field (but this effect is small as shown by the results in the main report). Viscous remanent magnetization is a remanent magnetization acquired with time, at a constant temperature. VRM is gradually acquired during exposure to weak magnetic fields and is acquired through thermal activation of domain walls.
2. If the ordnance detonates on or after impact, the fragments will acquire a new state of permanent magnetization. The shrapnel should

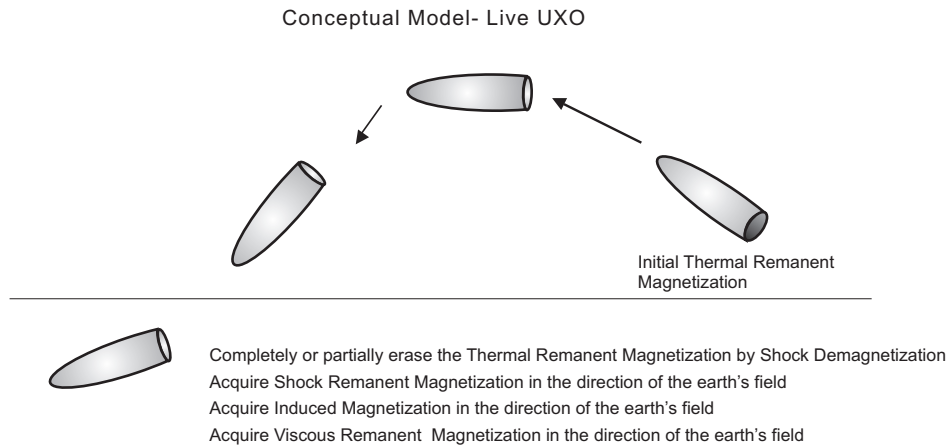


Figure 1: Magnetization of Live UXO.

have much different magnetic properties than UXO because they are subjected to a different (and typically larger) set of forces. On detonation, the metal casing of the bomb or projectile breaks apart. The resulting shrapnel are deformed and heated by the force of the explosion. The temperature of the blast could be higher than the steel's Curie temperature. Therefore there can be both shock and thermal changes to the magnetization.

3. If detonation is in the air, or at the surface, the shrapnel can be thrown a large distance from the point of impact. The orientation when the shrapnel comes to rest will have almost no relation to the direction of the ambient field at the time of the explosion. The direction of remanent magnetization will therefore be random.

In this report, we concentrate on understanding the first scenario.

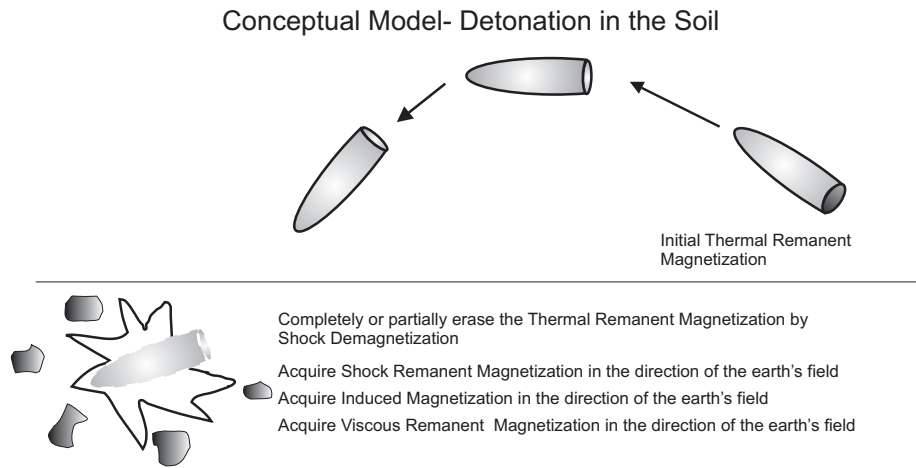


Figure 2: Magnetization of shrapnel when the ordnance detonates in the ground.

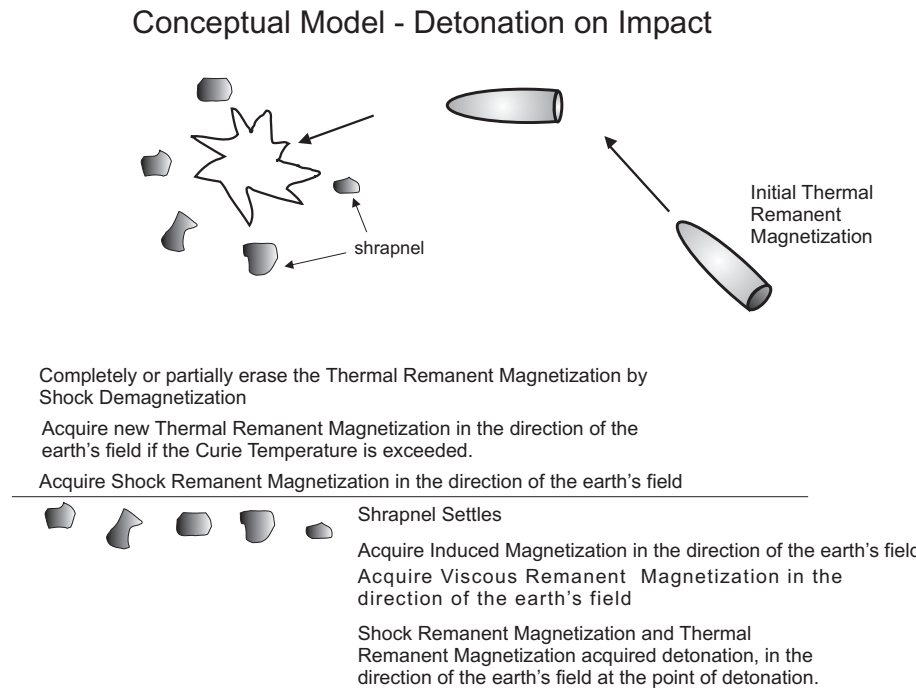


Figure 3: Magnetization of UXO shrapnel when the ordnance detonates above the ground.

2 Theory behind stress induced changes to magnetization

2.1 Stress

In the elastic regime, the change in length l of a material (of length l) when subjected to an applied force, F obeys, **Hooke's Law**,

$$F = YA \frac{\Delta l}{l}, \quad (1)$$

where A is the cross-sectional area of the material and Y is the Young's modulus. Using the fact that pressure σ is the force per unit area

$$\sigma = \frac{F}{A}, \quad (2)$$

and fractional change in length is strain, then

$$\text{Stress} = Y \times \text{Strain}. \quad (3)$$

Physically, stress is the externally applied pressure on a material and strain is how the material reacts [12].

A force applied in one direction can cause the material to change shape in the one of the directions perpendicular to the applied force. In addition, if the material is anisotropic then a force applied to the material as the orientation of that material is changed, can cause a different amount of strain. In that case, stress and strain will be tensors (S and e respectively) and will be related to other through the tensor of elasticity C [12]

$$S_{ij} = \sum_{k,l} C_{ijkl} e_{kl}. \quad (4)$$

2.2 Metals

The metal casing containing the explosive material in UXOs is what gives rise to a measurable magnetic signature. Metals are polycrystalline aggregates of many interlocking individual crystals or grains. The grain size varies depending upon the type of metal or alloy and is established during the melting and solidification of the metal in its manufacture. If cooled quickly, finer grains are produced. If cooled slowly, larger more stable grains are produced. Any additional manipulation done to the material, such as cold rolling etc, can change the crystal size and configuration of grains. Each

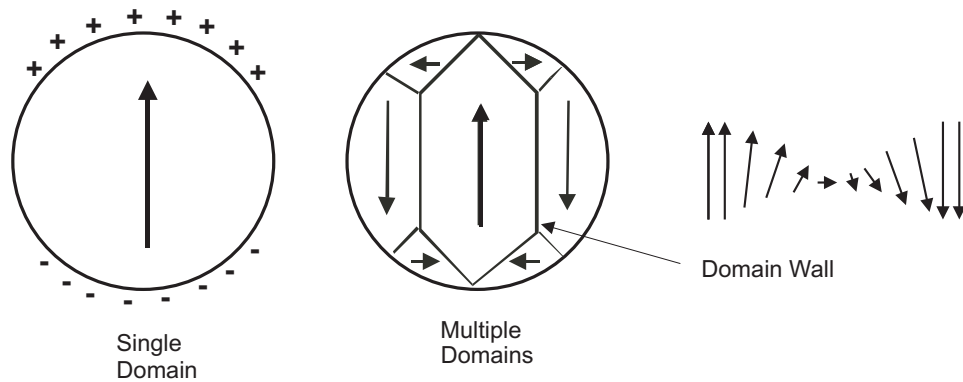


Figure 4: Magnetic domain structures.

crystal is made of individual cells repeated in a regular pattern to form 3-D lattice structures. Iron in its normal state is body-centered cubic and is a ferromagnetic material. Ferromagnetic solids have atoms with magnetic moments that interact strongly which results in large magnetizations.

2.3 Domain Theory and hysteresis

Metal is divided into regions called domains, within which the magnetic moments are aligned. Domains form to reduce what is known as magnetostatic energy, the energy caused by the repulsion of adjacent charges. In order to minimize this energy, magnetic domains form (Figure 4). As shown, the magnetization within each domain is equal to the saturation magnetization, M_s , but the net magnetization for the grain is less than the saturation magnetization. The magnetic moments within domain walls separating the domains spiral in direction.

The behavior of ferromagnetic materials below the Curie temperature, under the influence of a magnetic field, is described by the *hysteresis* loop (Figure 5). Application of a magnetic field to a multi-domain grain causes preferential growth of domains with magnetization parallel to the field. If the applied field is strong enough, domain walls are destroyed and magnetization reaches saturation M_s . On removal of the magnetizing field, domains reform and move back towards their initial position. The magnetization that remains after the field is removed is called remanent magnetization M_r . Because of lattice imperfections and internal strains, domain walls settle in an energy minima near their initial positions, and a remanent magnetization results.

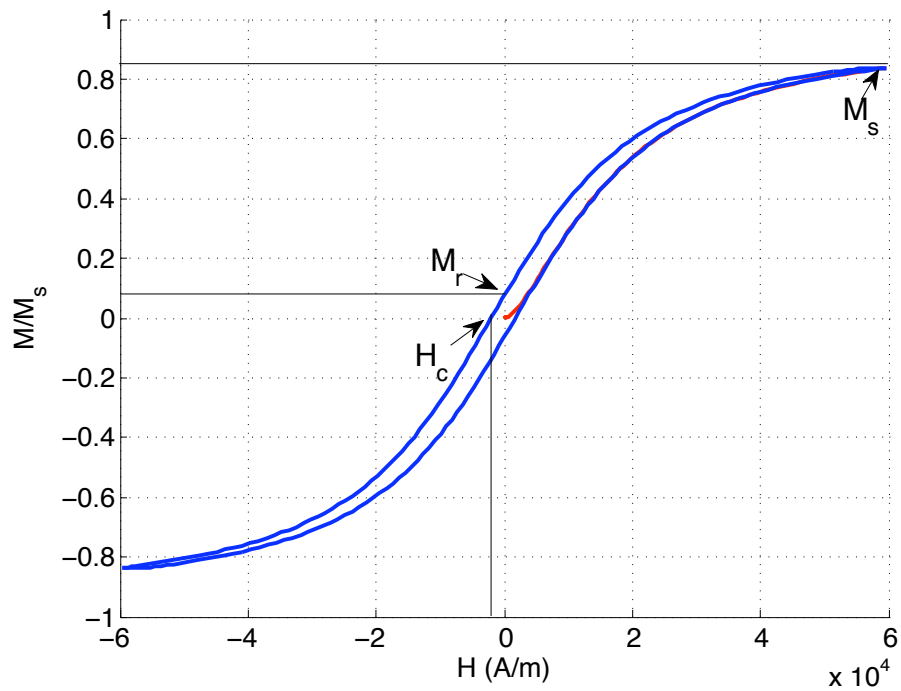


Figure 5: Illustration of important points on a hysteresis curve typical to iron such as saturation magnetization M_s , remanent magnetization M_r and coercive force H_c .

The coercive force, H_C , is the field necessary to move domain walls and change remanence so as to reduce magnetization to zero. Energy must be supplied to move the domain walls to overcome "wall pinning" which gives rise to magnetic hysteresis and coercivity.

Soft magnetic materials have a low remanent magnetization and typically low coercivity. They have a large grain size and well developed texture in which the grains tend to orient their crystal directions in some common direction. The texture is developed by rolling and recrystallizing. Hard magnetic materials resist changes in magnetization, and tend to have both large remanence and large coercivity. Their domain walls are pinned which prevents their movement by making it difficult for rotation of the magnetization direction to occur.

The main source of remanent magnetization for UXO's is *thermo-remnant magnetization* (TRM) which they acquire during the manufacturing of the metal casing. TRM is produced by cooling from above the Curie temperature in the presence of a magnetic field and acquired in metal during the melting and solidification process. The intensity of thermal remanence is linearly related to the intensity of the magnetic field applied during the cooling process of the metal through the Curie temperature. Above the Curie temperature the material is paramagnetic.

The full magnetization M is made up of different contributions as in [13]. These are the **anhysteretic magnetization**, the **reversible magnetization** and the **irreversible magnetization**. These are related by

$$M_{an} = M_s \mathcal{L} \left(\frac{H_e}{a} \right) \quad (5)$$

$$M_{rev} = c(M_{an} - M_{irr}) \quad (6)$$

$$M \equiv M_{tot} = M_{rev} + M_{irr}, \quad (7)$$

where \mathcal{L} is the Langevin function given as

$$\mathcal{L}(x) = \coth(x) + \frac{1}{x},$$

a is a field parameter and c is some coefficient determining the ratio of reversible to irreversible magnetizations. Possible mechanisms behind reversible magnetization are [13]

- bowing of domain walls between pinning sites
- planar domain wall movement in regions without pinning sites
- reversible rotations of domain walls with elastic strain

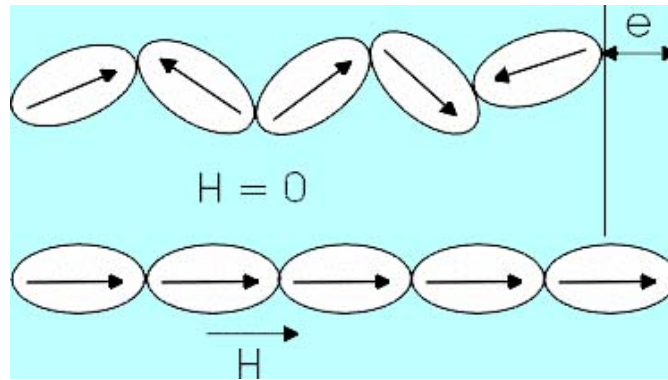


Figure 6: A schematic representing the elongation that can happen as a magnetic field is applied

2.4 Anisotropy

Magnetocrystalline anisotropy and shape anisotropy play an important role in the magnetization of ordnance. Magnetocrystalline anisotropy is the crystallographic directional dependence of ferromagnetism. The magnetocrystalline easy direction is the axis on which magnetic saturation, \mathbf{M}_s , is most easily achieved. Shape anisotropy is caused by magnetic charge distribution which opposes the magnetization of the grain. The field produced internal to the grain as a result of the magnetic charge distribution is called the internal demagnetising field. ΔeH is the energy needed to rotate \mathbf{M}_s from the perpendicular direction to the parallel direction. The microscopic coercive force is the magnitude of the magnetic field required to force the saturation magnetisation over this energy barrier, ΔeH .

Magnetostriction is a phenomenon whereby a shape of a ferromagnetic specimen changes during the process of magnetization [6]. The deformation is generally quite small with $\lambda = \Delta l/l$ on the order of 10^{-6} . Magnetostriction occurs because the crystal lattice inside each domain is spontaneously deformed in the direction of domain magnetization, thus resulting in a deformation of the specimen as a whole. A schematic of this effect can be seen in Figure 6. For anisotropy in iron, see [10], section 7.2, Fig 7.2. Recall that strain and stress are related. A change in shape of a material is referred to as strain which when multiplied by Young's modulus, will lead to stress or pressure. If the material experiences a change in shape due to magnetization, then the reverse effect must also be true. That is, applying pressure to a material must also affect its magnetization. This phenomenon is referred

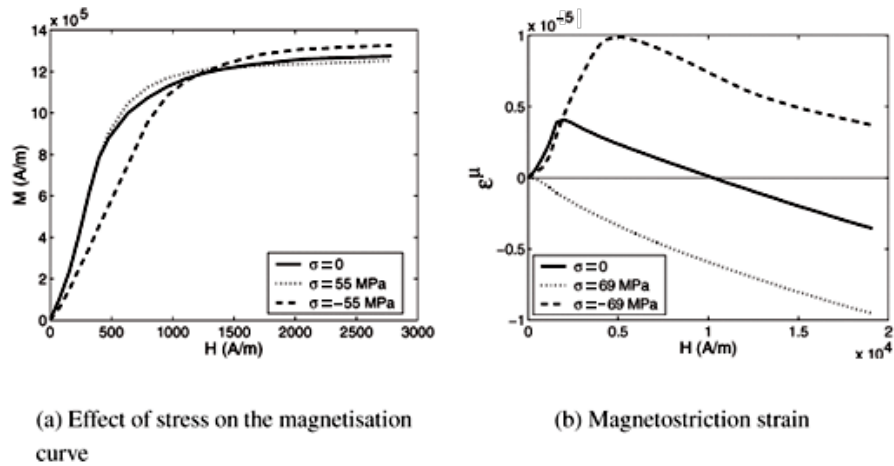


Figure 7: Qualitative illustration of the effect of stress on the magnetization and magnetostriction [10]

to as the **Villari effect** or the **magnetomechanical effect**.

The magnetostriction curve for iron is qualitatively shown in Figure 7. At first the magnetostriction is positive, hence compression (with the associated negative values of stress) leads to demagnetization. After a certain point, compression will once again magnetize a sample. Tension on the other hand, with the associated positive values of stress, will at first lead to an increase in magnetization and then demagnetization once the field of 1 kA/m is reached.

2.5 Effective Field

The concept of an effective field, H_e can be used to predict how magnetization of a specimen will change in the presence of an applied field H_{app} , or an applied stress σ . The Sablik-Jiles-Atherton model ([22] and [23]), relates the effective field to the applied and demagnetizing fields αM and the effective auxiliary field due to stress, H_σ through the equation,

$$H_e = H_{app} + \alpha M + H_\sigma,$$

The contribution of stress to the effective field is calculated as

$$H_\sigma = \frac{3\sigma}{2\mu_0} \left(\frac{d\lambda}{dM} \right)_T, \quad (8)$$

where μ_0 is the permeability of free space, M is the magnetization of the specimen and λ is the magnetostriction, all taken at a fixed temperature, T .

The approximate differential equation that models the $M - H$ hysteresis is given by

$$\frac{dM}{dH} = \frac{M_{an} - M_{irr}}{k\delta - \alpha(M_{an} - M_{irr})} + c \left(\frac{dM_{an}}{dH} - \frac{dM_{irr}}{dH} \right) \quad (9)$$

with $\frac{dM_{irr}}{dH}$ defined as

$$\frac{dM_{irr}}{dH} = \frac{M_{an} - M_{irr}}{k\delta - \alpha(M_{an} - M_{irr})},$$

and with $\frac{dM_{an}}{dH}$ as

$$\frac{dM_{an}}{dH} = M_s \left[-\frac{1}{a} \operatorname{cosech} \left(\frac{H_e}{a} \right)^2 + \frac{a}{H_e^2} \right]$$

Without any applied stress, the effective field due to stress, H_σ is set to zero. Computing hysteresis curves for steel leads to Figure 8. The two different branches of the curve are represented by $\delta = \pm 1$. This figure illustrates what happens to the hysteresis loop as parameters are varied. If the field constant is changed, then the slope of the curve varies. If the pinning constant k becomes larger, the area under the curve gets bigger. As the maximum field, H_{max} gets smaller, the hysteresis curves become smaller and smaller until they are approximately elliptic, minor curves.

Most constants for the calculation of the effective field can be found in literature as in [14], but the one thing that is unknown is the magnetostriction $\lambda(M)$. There have been several models proposed for this, such as the one in [22] and [23]. These range from simply making magnetostriction λ , as a polynomial which depends on magnetization M , or a more complicated version seen in the second paper. As seen in [22], the effective field due to stress in Equation (8), can be approximated using

$$H_\sigma(\sigma, M) = \frac{3}{2} \frac{\lambda}{\mu_0 M_s} \frac{M}{M_s} \sigma, \quad (10)$$

where the magnetostriction, λ , is approximated by using the models in Table 1.

For the third model, it should be noted that the asymmetry arises in the definition of λ_s which is given by

$$\lambda_s(\sigma) = \begin{cases} (\lambda_{s_0} - \lambda_{s_t})[1 - (\sigma/\sigma_t)^{1/2}] + \lambda_{s_t}, & \sigma \geq 0 \\ (\lambda_{s_0} - \lambda_{s_c})[1 - (\sigma/\sigma_t)^{1/2}] + \lambda_{s_c}, & \sigma \leq 0. \end{cases} \quad (11)$$

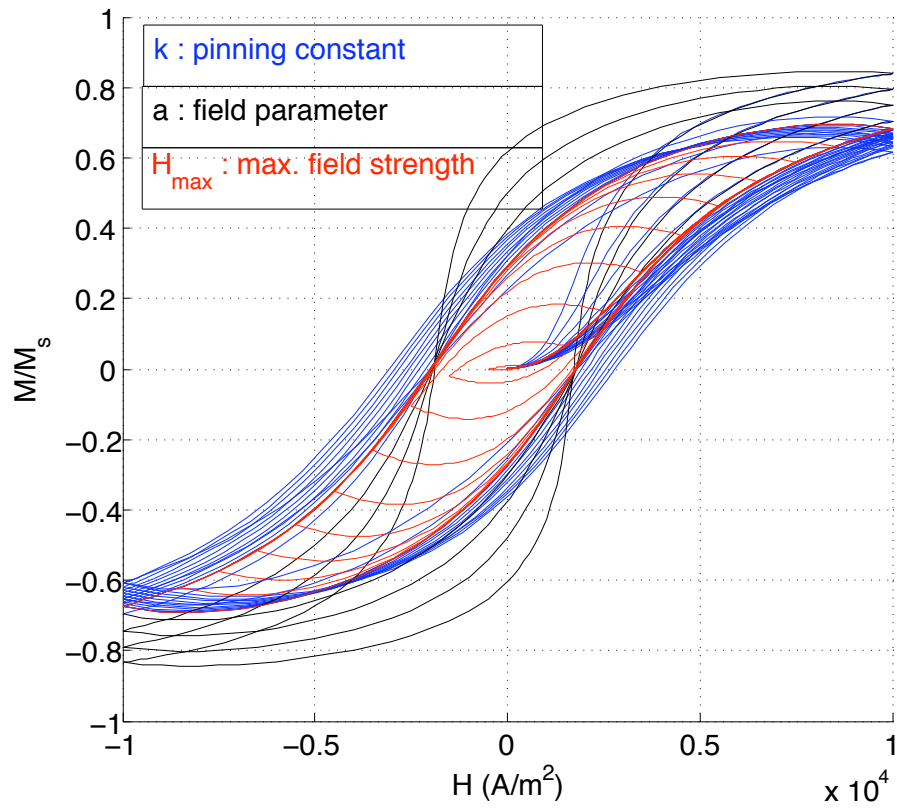


Figure 8: Different hysteresis curves given by varying parameters as seen in Equation (9) influence the shape.

Model	Corresponding Equation
Saturation magnetostriction	$\lambda = \lambda_{s_0}$
Constant stress dependence	$\lambda = \frac{3}{2}\lambda_{s_0}\left(\frac{M}{M_s}\right)^2$
Asymmetric stress dependence	$\lambda = \frac{3}{2}\lambda_s(\sigma)\left(\frac{M}{M_s}\right)^2$

Table 1: The models as shown in [22] for the magnetostriction of a material as it depends on the stress and the magnetization.

In the asymmetric model, the key is that there are two constants of magnetostriction, λ_c corresponding to compression and λ_t corresponding to tension. For more details, consult [22].

Another potential model was proposed by Sablik in [23]. In this one, working with Equation (8), the derivative term is approximated by using

$$\frac{d\lambda}{dM} = -\frac{a(\lambda_s/M_s)M_{an}}{[M_{an}^2 + b(M_s^2 - M_{an}^2)]^{1/2}}, \quad (12)$$

with a and b constant as given in the paper.

2.6 Attempt at modelling shock induced changes to magnetization

We attempted to harness the equations described above to create a quantitative model of the effects of stress on the magnetization of an ordnance item. We were unsuccessful in this endeavour, so rather than labouring through the details we will present an overview of the relevant literature we encountered. We hope that this literature review and the preceding discussion on phenomenology will be useful to anyone conducted additional research in this area.

3 Literature Review

3.1 Magnetostatic Principles in Ferromagnetism [3]

This book by Brown relates the work done by strain and work done by magnetism. This is one of the first heavily referenced books on the magnetic principles of ferromagnetism and takes the energetic approach. He distinguishes reversible and irreversible contributions. Also, he acknowledges that elasticity assumption of stress says long range forces can be expressed

as force per unit volume, but magnetism has surface concentrations and therefore breaks this assumption. Rigid body equations for work are considered. There is a discussion of how all forces interact (elastic, magnetic, electric) and that strain at constant field strength changes magnetization and change of the field at constant strain produces stress described by magnetostriction. However, this describes only change of strain with field at zero applied stress. This is followed by the Voigt approximation which describes this as product of strains and direction cosines, linear in strain but quadratic in cosines. This gives an explicit energy formula which can be minimized to find the equilibrium condition. Since magnetostrictive strain is not uniform, this must be corrected for the form effect. This is then concluded as being vague. Brown also notes the difference that magnetostrictive forces on 90° walls versus 180° walls and considers different anisotropy constants for iron depending on the x, y or z directions in the crystal lattice. At the end, Brown gives tables for demagnetizing factors for rectangular bars, cylinders and ellipsoids

3.2 Irreversible Magnetic Effects of Stress [4]

The main purpose of this seminal paper by Brown is to qualitatively explain the dependence of magnetization on stress. The applied stress in this case is tension and the magnitude is such that the ferromagnetic response is within the Rayleigh region. He states that once this goal is accomplished, then an experiment designed to test proposed theory can be done. This model for a change in magnetization J with respect to tension T contains, a polynomial dependence with constants derived from crystal and magnetic properties of the specimen

$$\delta J = \gamma_1 HT + \gamma_2 T^2.$$

Tests on experiments with a cylindrical steel rod agree with the theory. In order to extend this model to diminished alternating fields and stresses, an approach is outlined considering the probability that each part of the specimen receives a shock in some time interval.

3.3 Ferromagnetism and Ferromagnetic Domains [8]

The authors looked in detail into the ferromagnetic domains and then in films. There is a collection of experimental data and images of the domains for thin films. In this book, the magnetocrystalline energy is expressed in terms of directional cosines and anisotropy coefficients and as in the book by Brown, when minimized, this gives the preferred magnetization direction.

There are also constants for shape dependent properties given. Craik and Wood cover the domain structure for iron in particular and discuss internal stresses. They state that when the stresses are random, they will affect the direction and magnitude of the anisotropy. Also, they note that in a well-annealed material, the minimum strains σ are proportional to the change in shape of material (known as magnetostriction) λ multiplied by the Young's modulus Y ,

$$\sigma = \lambda_s Y.$$

This book covers mostly experimental domain wall observations with diagrams and given constants.

3.4 Magnetization Changes Induced by Stress in a Constant Applied Field [9]

The authors here used experimental measurements basing the proposed theory on Brown's work where

$$H_\sigma = \frac{3 \lambda \sigma}{2 M_s},$$

in order to extend it to specimens in higher fields experiencing both compression and tension. These specimens were nickel, mild steel as well as isotropic and cube textured silicon iron. The experimental procedures are outlined in great detail in the paper and from these experiments, magnetization curves were obtained. The most important features of the curves include a difference between tension and compression measurements, the opposite roles of tension and compression in nickel and steel and a dependence of stress on applied field as well as effects on permeability. An analysis of the different domain wall types including the concept of how 90° walls are affected by stress and that 180° are not. It is concluded that the dependence of magnetization on stress is not simply explained by domain wall motion, but also permanent change in domain structure.

3.5 Physics of Ferromagnetism [6]

Very comprehensive and relatively advanced book. It covers magnetostriction and anisotropy. It also has detailed illustrations of magnetization based on domain theory of magnetism and includes concepts such as Kaya's rule not found anywhere else. It is a very heavily referenced manual.

3.6 Introduction to Magnetism and Magnetic Materials [13]

An introductory level book structured in the way of questions and answers. It was mostly used to supplement the papers on models which incorporate stress into hysteresis.

3.7 Introduction to Magnetic Materials [10]

This book gives a good introduction to all types of magnetic materials, and also discussing magnetic anisotropy in detail. It discusses how to determine anisotropy from experiment by fitting to magnetization curves and includes some of these curves such as the magnetization for an iron crystal in different crystal axis directions. It also discusses anisotropy constants and their temperature dependence as well as shape anisotropies and why is it easier to magnetize a specimen along a long axis than along a short axis. Cullity computes the magnetostatic energy by considering that the non-symmetrically shaped object in zero field will still have an applied demagnetizing field and therefore energy of

$$E_{ms} = -\frac{1}{2}H_dM.$$

It can then be compared to the potential energy for a magnet

$$E_p = -H_aM.$$

A lengthy discussion on magnetostriction and effects of stress follow. There is a comprehensive overview of magnetostriction for specific materials and dependence on field and crystal axis directions. He discusses the physical origins of magnetostriction and distinguishes this from the form effect. Cullity also discusses the effect of stress on magnetic properties, relates magnetostriction and magnetic behaviour under stress by saying the latter is the inverse. He shows the effects of tensile (+) stress and how it lowers M_s and that compressive stress (-) on iron leads to higher M_s . He also introduces magnetoelastic energy as

$$E_{me} = \frac{1}{2}\lambda\sigma \sin^2 \theta$$

where θ is the angle between the magnetization axis M and stress σ . A section on how stress affects magnetostriction and Young's modulus is included.

Some qualitative properties for low and high field magnetizations are discussed including the Rayleigh region. He explains that plastic deformation can induce magnetic anisotropy in that it makes magnetization more

difficult: the hysteresis loop rotates clockwise and has a higher coercivity, larger hysteresis loss and smaller total magnetization. This is caused by the increasing number of dislocations and lattice defects that impede domain wall movement and rotation. Also, other differently shaped hysteresis curves are discussed with associated properties.

3.8 Origins of the Magnetomechanical Effect [5]

The paper focusses on mostly qualitative features in stress affected hysteresis curves in order to explain theoretically what happens. The main experiment is done on a cruciform of annealed mild steel. Applied stresses range from -120 MPa to $+120$ MPa and maximum applied field strength of a few kA/m. It was found that the dominant features in the hysteresis curves were two coincident points for the different stress and also a visible "kink" that occurs at those coincident points. This data was verified with secondary experiments using a rod of mild steel with lower applied fields and a nickel specimen. The steel rod showed the same coincident points, however the nickel had these points in a different area of the graph.

Theory was suggested to explain this on a microscopic level. It is known that ferromagnetic materials are made of grains and to achieve saturation magnetization, both reversible and irreversible contributions play a role. The applied stress distorts the crystal lattice since relative separations of atoms change and therefore the angles between easy and hard directions change. In order to reach saturation, the moments need to rotate from the easy direction towards the direction of applied field. When the axes shift under stress, the energy balance between anisotropy energy and exchange energy change which contributes to the magnetomechanical effect. Stress affects 90° walls, reducing the magnetization by compression and increasing the favourable domains by tension. The coincident points are explained as the point where the net field is not sufficient enough to rotate the magnetic moments away from their easy axes. The response of the material to stress is nonlinear and the material will fail at high stresses. It is shown that stress-induced anisotropy is equal to magnetocrystalline anisotropy if stress is 105 MPa for nickel and 4600 MPa for iron.

3.9 Numerical Determination of Hysteresis Parameters for the Modeling of Magnetic Properties Using the Theory of Ferromagnetic Hysteresis [14]

This paper is mostly concerned with finding constants to describe hysteresis curves. It relies on the previously solved hysteresis ODE and shows how the model parameters can be obtained from experimental data. The total differential susceptibility is shown to be

$$\frac{dM}{dH} = (1 - c) \frac{M_{an} - M_{irr}}{k\delta - \alpha(M_{an} - M_{irr})} + c \frac{dM_{an}}{dH}.$$

Some sample solutions are plotted in the paper with different parameters for $M_s, a, k, \alpha,$ and c . These can be obtained from the experimental parameters such as the different differential susceptibilities $\chi'_{in}, \chi'_{an}, \chi'_{M_r}$, the coercive field H_c , the remanence M_r and the reference point at the tip of the hysteresis H_m, M_m . Taking the proper limits and derivatives, the different relationships between model parameters and experimental data are determined and given as equations in the paper. Sample experimental magnetic properties of different types of steel as well as sample model parameters are given in tables.

3.10 Modeling of the Magnetomechanical Effect: Application of the Rayleigh Law to the Stress Domain [15]

This work builds on the work done by Craik and Wood. Using the expression derived from thermodynamics for the effective field due to stress

$$H_\sigma = \frac{3}{3} \frac{\sigma}{\mu_0} \left(\frac{d\lambda}{dM} \right),$$

the expression for the effective field is derived to be dependent on the angle between axis of applied stress and axis of the magnetic field as

$$H_{eff} = H + \alpha M + \frac{3\gamma_1\sigma_0}{\mu_0} (\cos^2 \theta - \nu \sin^2 \theta) M$$

where γ_1 is a model parameter of magnetostriction. This results in a model for the change in magnetization with respect to stress including two model parameters α and β ,

$$\Delta M = 2M_s(\alpha|\sigma| + \beta\sigma^2).$$

The claim is that this agrees better with experimental observation. A new differential equation for hysteresis including stress is derived as

$$\frac{dM}{dH} = \frac{1}{\epsilon^2}(1 - c)(M_{an} - M_{irr})(\sigma \pm \eta E) + c \left(\frac{\sigma}{E} \pm \eta \right) \frac{dM_{an}}{d\sigma}.$$

3.11 Model for the Effect of Tensile and Compressive Stress on Ferromagnetic Hysteresis [22]

The results of this paper were used extensively throughout the report. The authors use the hysteresis model for ferromagnets and extend it to include the effects of stress using the fact that tensile stress and positive magnetostriction leads to an increase in magnetization whereas compressive stress and positive magnetostriction leads to a decrease in magnetic induction and adds more curvature. Families of hysteresis curves were drawn for a steel sample with hardness of 53 for three values of stress, -40 ksi , 0 and 40 ksi and fields of up to 80 Oe . Using the effective field model given by

$$H_e = H + \alpha M + H_\sigma,$$

where

$$H_\sigma = \frac{3}{2} \frac{\lambda}{\mu_0 M_s} \frac{M}{M_s} \sigma,$$

three models for the magnetostriction were proposed. These are the ones used in this report, Table 1. Representative curves are the plotted for the different models and the asymmetric behaviour under tension and compression is discussed since experimentally, it is observed that the hysteresis curve has a greater curvature under compression than under tension.

3.12 A Model for Asymmetry in Magnetic Property Behavior Under Tensile and Compressive Strain in Steel [23]

This paper uses the known observation that a magnetized material under compression and tension does not behave the same way, known as the Villari effect, and by incorporating two different theories, Sablik builds a new model to illustrate this. A stress demagnetization term of the form

$$D_\sigma M_i,$$

is incorporated into the effective field such that

$$H_e = H + \alpha M_a - D_\sigma M_a + \frac{3\sigma}{2\mu_0} \frac{d\lambda}{dM_a}.$$

The stress demagnetization term which has previously not been physically explained is pedagogically accounted for as the alignment of grains leading to an asymmetry in the demagnetizing factor under tension and compression like that of a cylinder. Another multiplicative term is included so that a maximum Villari effect can be achieved and this is done by using a Gaussian term multiplying the saturation magnetostriction in the effective field due to stress H_σ . Solving the new ODE for hysteresis, figures are shown that include coercivity and remanence with respect to stress which show that the slope increases if the demagnetization term is present under compression are obtained and discussed.

3.13 Demagnetizing Factors of General Ellipsoid [18]

This paper is a good reference for demagnetizing factors of ellipsoids with three different axes. This is done by using the fact that when a ferromagnetic body with field J_i is placed in an external magnetic field H_o , the magnitude and direction inside the body, H_i , will vary according to

$$H_i = H_o - N_i J_i.$$

The demagnetizing factor N_i is determined by the ratio of axes and calculated using Poisson's equations. Formulas for simple cases of oblate and prolate ellipsoids are given in the paper. Also, this paper includes table and figures of demagnetizing factors for more complicated geometries.

3.14 A Review of Investigation of the Magnetization of Steel Due to the Application of Stress [20]

This thorough review paper of magnetomechanical effect consist mostly of experimental observations for different types of steel. A strong emphasis is put on the cyclic application of stress to specimens. It starts with basic common notation and outlines some ferromagnetic phenomena with schematic diagrams as well as key contributing experiments and experimenters who helped understand the interaction between stress and magnetization. The main focus of the paper is to distinguish reversible and irreversible effects.

3.15 Effects of Stress on the Magnetization of Steel [1]

The authors applied a series of stresses to a 1% manganese steel at low fields. It was observed that this caused the magnetic response to approach that of an anhysteretic material. The change in magnetization is proportional to

the amount of stress, but with a strong dependence on the initial conditions. The physical explanation is that motion of domain walls is impeded by pinning sites. Internal stresses affect domain wall energy and change the amount of inclusions and voids. The anhysteretic is also dependent on stress experienced by the sample. At low fields where the domain wall motion dominates, the change in magnetization was found to be independent of whether the stress was compressive or tensile. In this paper, plots are presented which illustrate the change in flux density with respect to stress at various points, with different stresses and also initial conditions.

3.16 On the Rayleigh Law of Magnetization: a New Mathematical Model of Hysteresis Loops [11]

One of the goals of the paper is to first clearly outline the Rayleigh law for magnetic hysteresis. This was the purpose for which we used the paper. It then proceeds to formulate a model that incorporates experimental parameters to describe the symmetric behaviour of a magnetic specimen subject to a weak ac field. It then generalizes the model to an asymmetric model if the specimen is also under the influence of a biasing dc field.

3.17 Other papers

Studies have looked at the effects of shock on magnetization and found that within low pressure ranges of a few kilobars, the results of static experiments are similar to those of dynamic experiments [19, 7, 21]. The measurements of [21] on the shock demagnetization of nickel ferrites showed an apparent complete destruction of the spontaneous magnetization of the material at all shock pressures between 43 and 430 kbar. [19] showed that in the pressure range of 1 to 10 kbar, thermoremanent magnetization can be demagnetized by shocking. With increasing shock pressures, progressively higher coercivity fractions are demagnetized. He stated that it is probable that existing theories for static experiments can be applied to dynamic experiments, taking into account the short duration of the stress impulse and the effect of repeated shocks. Also, in the stress range of 2.5 to 10 kbar, both irreversible displacements of 90 degree domain walls and irreversible rotation of spontaneous magnetization contribute to changes of the remanent magnetization. The work of [19, 21, 2, 17] support the theory that anisotropic strain resulting from shock impact may induce a magnetic anisotropy which changes the remanent magnetization.

The work of [2, 24] examined how shock can induce a uniaxial magnetic

anisotropy in the material that becomes the easy direction of magnetization. [24] measured the shock-induced reduction in the component of magnetization of polycrystalline yttrium iron garnet (YIG) along the direction of an applied field by applying a shock in the direction perpendicular to the field. The shock wave generates a uniaxial magnetic anisotropy in the material and this direction becomes the easy direction of magnetization. The reduction of the magnetization along the applied field arises from the rotation of the magnetization toward the easy direction.

[17] conducted experiments to investigate the domain-wall theory of piezo- and shock remanent magnetization of rocks. They developed a simple model of configuration of magnetic domains of magnetic minerals under the effect of inverse magnetostriction. The results supported the theory that the total volume of domains with direction of spontaneous magnetization perpendicular to the axis of compression increases with an increase of compression. A release of the compression from a sample in the presence of a magnetic field along the compression axis should result in a preference of orientation of spontaneous magnetization of domains towards the direction of the magnetic field. [16] showed that isothermal remanence carried by a rock can be substantially reduced, and a remanence proportional to the ambient field can be acquired at pressures comparable to those suffered by a rock when struck by a geologic hammer. The shock remanent magnetization acquired in the presence of a magnetic field was very large compared with the ordinary isothermal remanent magnetization. The application of a mechanical shock of very short time duration on a sample cannot achieve the completion of the shock effect represented by the effect of the pressure peak in the shock momentum, but when the same shock operations are repeated, the resultant effect approaches the completed final state in an exponential form.

References

- [1] D. L. Atherton and D. C. Jiles. Effects of stress on the magnetization of steel. *IEEE Transactions on magnetics*, 19(5):2021(3), 1983.
- [2] I. C. Bartel. Theory of strain-induced anisotropy and the rotation of the magnetization in cubic single crystals. *J. Appl. Phys.*, 40(2):661–669, 1969.
- [3] William F. Jr. Brown. *Magnetostatic principles in ferromagnetism*, volume 1. North-Holland Publishing Company, 1962.
- [4] William Fuller Jr. Brown. Irreversible magnetic effects of stress. *Physical Review*, 75(1):147(8), 1948.
- [5] D.P. Bulte and R. A. Langman. Origins of the magnetomechanical effect. *Journal of Magnetism and Magnetic Materials*, 251:229(14), 2002.
- [6] Soshin Chikazumi. *Physics of Ferromagnetism*. Oxford Science Publications, 1997.
- [7] S. M. Cisowski and M. Fuller. The effect of shock on the magnetism of terrestrial rocks. *J. Geophys. Res.*, 83(B7):3441–3458, 1978.
- [8] D. J. Craik and R. S. Tebble. *Ferromagnetism and ferromagnetic domains*, volume 4. North-Holland Publishing Company, 1965.
- [9] D. J. Craik and M. J. Wood. Magnetization changes induced by stress in a constant applied field. *Journal of Physics D. : Applied physics*, 3:1009(8), 1970.
- [10] B.D. Cullity and D.C. Graham. *Introduction to Magnetic Materials*, volume 2. Wiley, IEEE Press, 2009.
- [11] Ponomarev Yu. F. On the Rayleigh law of magnetization: a new mathematical model of hysteresis loops. *The physics of metals and metallography*, 104(5):469(9), 2007.
- [12] Richard P. Feynman, Robert B. Leighton, and Matthew Sands. *The Feynman Lectures on Physics*. Addison-Wesley Publishing Company Inc., 1964.
- [13] David Jiles. *Introduction to Magnetism and Magnetic Materials*. Taylor and Francis, 1998.

- [14] D.C. Jiles. Numerical determination of hysteresis parameters for the modeling of magnetic properties using the theory of ferromagnetic hysteresis. *IEEE Transactions on magnetics*, 28(1):27(9), 1992.
- [15] L. Li and D.C. Jiles. Modeling of the magnetomechanical effect: application of the Rayleigh law to the stress domain. *Journal of Applied Physics*, 93(10):8480(3), 2003.
- [16] T. Nagata. Introductory notes on shock remanent magnetization and shock demagnetization of igneous rocks. *Pure. Appl. Geophys.*, 89:159–177, 1971.
- [17] T. Nagata and B. J. Carleton. Notes on piezo-remanent magnetization of igneous rocks II. *J. Geomag. Geoelectr.*, 29:427–445, 1969.
- [18] J. A. Osborn. Demagnetizing factors of the general ellipsoid. *Physical Review*, 62(11):351(7), 1945.
- [19] J. Pohl, U. Bleil, and U. Hornemann. Shock magnetization and demagnetization of basalt by transient stress up to 10 kbar. *J. Geophys. Res.*, 41:23–41, 1975.
- [20] I. M. Robertson. A review of investigations of the magnetization of steel due to the application of stress. *Materials Forum*, 15:117(14), 1991.
- [21] E. B. Royce. Anomalous shock induced demagnetization of nickel ferrite. *J. Appl. Phys.*, 37(11):4066–4070, 1966.
- [22] H. Sablik, M.j. Kwun, Burkhardt G. L., and D.C. Jiles. Model for the effect of tensile and compressive stress on ferromagnetic hysteresis. *Journal of Applied Physics*, 61(8):3799(3), 1987.
- [23] M. J. Sablik. A model for asymmetry in magnetic property behavior under tensile and compressive stress in steel. *IEEE Transactions on magnetics*, 33(5):3958(3), 1997.
- [24] J. W. Shanner and E. B. Royce. Effect of shock on the magnetization of yttrium iron garnet. *J. Appl. Phys.*, 39:492–500, 1968.